EPRI

Electric Power
Research Institute

Topics:
Transmission towers
Transmission lines
Foundations
Soils
Design
Testing

EPRI EL-3777
Project 1493-1
Final Report
November 1984

Load Transfer Mechanisms in Rock Sockets and Anchors

Prepared by
Cornell University
Ithaca, New York

REPORT SUMMARY

SUBJECTS	Towers / Transmission: Overhead lines
TOPICS	Transmission towers Transmission lines Foundations Soils Design Testing
AUDIENCE	Transmission managers and engineers

Load Transfer Mechanisms in Rock Sockets and Anchors

This modeling effort provides a basic understanding of load transfer mechanisms in rock sockets and anchors. The work focuses on geotechnical problems and shows the sensitivity of socket behavior to changes in key parameters.

BACKGROUND Possible failure modes for rock sockets and anchors are classified as either structural or geotechnical concerns. Structural aspects are adequately addressed by current codes and practices, so the emphasis here was on developing models to evaluate the geotechnical problem.

OBJECTIVE To develop a fundamental understanding of load transfer mechanisms in rock sockets and anchors.

APPROACH Tendon tensile failure and tendon pullout from grout are structural failure mechanisms. Although they are adequately covered by current codes and practices, researchers reviewed those codes and practices to provide a complete treatment of the subject. Grout-rock interface failure and rock mass uplift, focused on in this study, are geotechnical failure modes. The researchers examined the progression of grout-rock interface failure from elastic to secondary to residual stages. And through an analysis of anchor pullout tests, they investigated the transition in rock mass uplift failures, from fracture and cracking to interface slip. Analysis of both geotechnical failure modes is based on a combination of original concepts and summaries of existing methods. Field load tests were used to evaluate the resulting model.

RESULTS The emphasis of this work was on developing models to evaluate the geotechnical problems in rock sockets and anchors. In the case of grout-rock interface failure, equations and data were available to evaluate capacity and behavior in the three failure stages. The model developed in this project accurately predicted this mode of failure. However, researchers could not evaluate model accuracy for the rock mass–uplift failure mechanism because of limited test data.

EPRI PERSPECTIVE This study demonstrates that rock sockets and anchors are amenable to a more rational analysis than current empirical practice suggests. The information presented advances design practice toward the goal of more efficient

and more cost-effective transmission tower foundations. Related to this research are two other EPRI reports, EL-2870 and EL-3771. The first report contains a state-of-the-art review and establishes a unified model for foundation design subject to uplift/compression loading. The second report summarizes more than 800 foundation load test histories, which were used in a critical evaluation of the proposed model. The research described focused on drilled shaft foundations because they are the most widely used by the utility industry and because of the availability of field test data on them. This report broadens the scope of EPRI's foundation research programs to include rock sockets and anchors. Analysis of spread-type foundations is forthcoming.

PROJECT RP1493-1
EPRI Project Manager: Vito J. Longo
Electrical Systems Division
Contractor: Cornell University

For further information on EPRI research programs, call
EPRI Technical Information Specialists (415) 855-2411.

ORDERING INFORMATION EPRI EL-3777, Final Report, November 1984, 102 pages.

EPRI Members If this report is not available from your company libraries or your Technical Information Coordinator, you can order it from

Research Reports Center
P.O. Box 50490
Palo Alto, CA 94303
(415) 965-4081

Nonmembers You can order this report in print or microfiche from Research Reports Center.

Price: $13.00 Overseas price: $26.00
(California residents add sales tax.)
Payment must accompany order.

Load Transfer Mechanisms in Rock Sockets and Anchors

EL-3777
Research Project 1493-1

Final Report, November 1984

Prepared by

CORNELL UNIVERSITY
Geotechnical Engineering Group
Hollister Hall
Ithaca, New York 14853

Authors
K. A. Pease
F. H. Kulhawy

Principal Investigator
F. H. Kulhawy

Prepared for

Electric Power Research Institute
3412 Hillview Avenue
Palo Alto, California 94304

EPRI Project Manager
V. J. Longo

Overhead Transmission Lines Program
Electrical Systems Division

ORDERING INFORMATION

Requests for copies of this report should be directed to Research Reports Center (RRC), Box 50490, Palo Alto, CA 94303, (415) 965-4081. There is no charge for reports requested by EPRI member utilities and affiliates, U.S. utility associations, U.S. government agencies (federal, state, and local), media, and foreign organizations with which EPRI has an information exchange agreement. On request, RRC will send a catalog of EPRI reports.

Research Categories: Towers
Transmission: Overhead lines

NOTICE

This report was prepared by the organization(s) named below as an account of work sponsored by the Electric Power Research Institute, Inc. (EPRI). Neither EPRI, members of EPRI, the organization(s) named below, nor any person acting on behalf of any of them: (a) makes any warranty, express or implied, with respect to the use of any information, apparatus, method, or process disclosed in this report or that such use may not infringe privately owned rights; or (b) assumes any liabilities with respect to the use of, or for damages resulting from the use of, any information, apparatus, method, or process disclosed in this report.

Prepared by
Cornell University
Ithaca, New York

ABSTRACT

This study presents a comprehensive analysis of rock socket and anchor behavior, which includes the failure mode, capacity, and deformations. The methods of analysis were obtained from a combination of original concepts and summaries of preexisting methods. The original concepts are based on both theoretical considerations and observations of actual socket behavior. The data used for both analytical and verification purposes were obtained from published sources. The results show that rock sockets and anchors can fail by any one of four modes, including: tensile failure of the tendons, pullout of the tendons from the grout, grout-rock interface slip, and rock mass uplift. Only the latter two are geotechnical problems investigated in detail.

Grout-rock interface failure is outlined as a progression of behavior from elastic, to secondary, and finally residual stages. The elastic stage is characterized as an intact system in which displacements develop from elastic deformations of the foundation and rock mass. In comparison, the secondary stage is characterized by a relative displacement between the foundation and the rock mass. Finally, the residual stage results from large displacements between the foundation and rock mass, and is characterized by complete degradation of the interface between the foundation and rock mass. Equations and data are presented to evaluate the behavior in each stage.

For shallow foundations installed in highly fractured rock masses, failure can be by rock mass uplift. In this case, failure is associated with cracking and loosening of the rock mass which can be approximated by a cone failure. This mode gradually transitions to the grout-rock interface failure mode with increasing depth.

ACKNOWLEDGMENTS

The authors appreciate the assistance of several people during the conduct of this research and wish to acknowledge their efforts. T. D. O'Rourke of Cornell University was an advisor, constructive critic, and reviewer throughout this study, and made many valuable contributions.

Several colleagues graciously responded to a request for review and evaluation of the first draft of this report. These included: J. I. Adams, Ontario Hydro; J. C. Burton, San Diego Gas and Electric; M. A. Mahtab, Columbia University, T. E. Rodgers, Jr., Virginia Electric and Power Company; and J. P. Stewart, Syracuse University.

The EPRI project manager during the research was P. G. Landers, while the EPRI project manager during the final report stage was V. J. Longo. L. Donley typed the text and A. Avcisoy drafted the figures.

CONTENTS

ILLUSTRATIONS

Figure		Page
3-2	Determination of k_1	3-3
3-3	Shear Stress-Displacement Curve of Best Fit	3-5
3-4	Prediction of Socket Behavior Using Initial Assumptions	3-7
3-5	Comparison of Back-Calculated Dilations with Predictions Based on Equation 2-16	3-8
3-6	Modeling Dilations for Shear Socket M3 Using Equation 3-1	3-10
3-7	Shear Stress-Displacement Curve for Best Fit for Shear Socket M3	3-10
3-8	Prediction of Socket Behavior and Capacity for Tests by Webb and Davies	3-11
3-9	Sensitivity of Prediction to Changes in Normal Stiffness, k_n	3-13
3-10	Sensitivity of Prediction to Changes in Initial Dilation Angle, i_o	3-13
3-11	Sensitivity of Prediction to Changes in Asperity Half Wave Length, λ	3-14
3-12	Sensitivity of Prediction to Changes in Empirical Coefficient, k_5	3-14
3-13	Sensitivity of Prediction to Changes in Rock Strength Component, ϕ_b	3-15
3-14	Sensitivity of Prediction to Changes in Empirical Coefficient, k_1	3-15
4-1	Axial Stress Distribution Along Anchor 6	4-4
4-2	Axial Stress Distribution Along Anchor 53	4-5
4-3	Vertical Cross-Section of Failed Anchor 3	4-6
4-4	Rock Surface Fracture Pattern for Anchor 6	4-7
4-5	Rock Surface Fracture Pattern for Anchor 53	4-8
A-1	Mesh for Socket with Length/Radius = 2.0	A-2
A-2	Node Numbers for Socket with Length/Radius = 2.0	A-2
A-3	Mesh for Socket with Length/Radius = 4.0	A-3
A-4	Node Numbers for Socket with Length/Radius = 4.0	A-3
B-1	Determination of k_1 for Test SM2	B-2
B-2	Shear Stress-Displacement Curve for Best Fit for Test SM2	B-2
B-3	Determination of k_1 for Test SM3	B-2
B-4	Shear Stress-Displacement Curve of Best Fit for Test SM3	B-3
B-5	Determination of k_1 for Test SM4	B-3

TABLES

SYMBOLS

ENGLISH LETTERS - UPPER CASE

B - bond, a chemical linkage

D - foundation diameter

E_g, E_m, E_r - Young's modulus for grout, rock mass, rock material

H - depth of embedment

I_ρ - elastic settlement influence factor

JRC - Barton's joint roughness coefficient

K_E - stiffness ratio

L - foundation length

P - applied load

Q - stress transfer factor

RMR - Bieniawski's rock mass rating

RMS - root-mean-square of asperity height

RQD - rock quality designation

SD_h - standard deviation of asperity height

SD_i - standard deviation of asperity angle

ENGLISH LETTERS - LOWER CASE

a_r - area reduction ratio

b - empirical constant

c_j - shear intercept for intact rock

h_a - average asperity height

h_m - total asperity height

i_a - average asperity angle

i_o - initial dilation angle

k_n - normal stiffness

k_1, k_2, k_3, k_4, k_5 - empirical coefficients

q_u - uniaxial compressive strength

r - foundation radius; correlation coefficient

u - dilation

u_c - limiting dilation

$\dot{u}$ - rate of dilation

y - vertical distance

Δy - vertical displacement

z_2 - root-mean-square of asperity height

GREEK LETTERS

α - average unit side resistance reduction factor

η - degree of interlocking

λ - half wave length of asperities

ν_g, ν_m, ν_r - Poisson's ratio for grout, rock mass, rock material

ρ - elastic settlement

σ_n - normal stress

σ_T - transition stress

σ_y - vertical stress in foundation

σ_1 - major principal stress

σ_3 - minor principal stress

τ - shear stress

ϕ_a - apparent friction angle for sliding

ϕ_b - base friction angle

ϕ_i - friction angle for intact rock

ϕ_r - apparent friction angle from tooth strength

ψ_o - initial slope of stress path

SUMMARY

This report is the fourth prepared for the Electric Power Research Institute (EPRI) on Research Project 1493, "Uplift/Compression Transmission Line Structure Foundation Research". The general objectives of this research are the development and implementation of rational analysis and design procedures for the foundations of transmission line structures.

In this report, the emphasis is on developing a fundamental understanding of load transfer mechanisms in rock sockets and anchors. A rational analytical model is developed which incorporates actual rock mass behavior characteristics. This model was tested against the limited available field data, with encouraging results.

CURRENT DESIGN METHODS

Rock sockets and anchors can fail in four modes: (1) tensile failure of the tendons, (2) pullout of the tendons from the grout, (3) grout-rock interface failure, and (4) rock mass uplift. Current design practices for all four modes are reviewed, and it is noted that criteria for modes 1 and 2, which are structural concerns, are developed adequately in appropriate steel and concrete codes. Criteria for modes 3 and 4, which are geotechnical concerns, are predominantly empirical at this time.

GROUT-ROCK INTERFACE FAILURE

The mode 3 mechanism is examined in detail and it is shown that interface failure is a function of displacement, and progresses from elastic, to secondary, and finally residual stages. The elastic stage can be evaluated using closed-form or finite element solutions. The secondary stage is characterized by relative displacement between the foundation and rock mass. In this stage, the capacity is a function of normal stresses developed by dilations, which are caused by irregularities along the grout-rock interface. The residual stage is a limiting case developed at very large deformations. Existing data are used to assess the necessary analysis parameters.

ROCK MASS UPLIFT

Very shallow anchors and sockets installed in highly fractured rock masses may fail in rock mass uplift. In these cases, failure is associated with cracking and loosening of the rock mass. However, there is a gradual transition from the uplift to the interface failure modes. Existing data on the uplift mode are very limited, and therefore only empirical criteria can be employed at present.

CONCLUSIONS

This study demonstrates that rock sockets and anchors can be evaluated in a more rational manner than current empirical practice suggests. Although further data are needed to establish well-defined confidence limits, it is clear that our understanding of how rock sockets and anchors behave is improved.

This information represents an advance to current design practice and will assist engineers in the analysis and design of more cost-effective foundations systems.

Section 1

OVERVIEW AND DESIGN

Foundations of engineered structures are often constructed in rock masses. The common foundation types include anchors, which behave as tension members, and sockets, which can be used for tension, compression, and other loading modes. Currently, the design of anchors and sockets is based primarily on empirical relations developed from summaries of load test results. Uncertainties in these methods necessitate the use of relatively high safety factors. More economical designs can be used only if an on-site testing program is undertaken.

Most of the available literature has focused on the behavior of specific components of anchor and socket systems, and few studies address the interaction of all components. This study builds upon the available theoretical and experimental work to present a comprehensive analysis of the behavior and capacity of rock sockets and anchors. Where possible, the analysis is compared directly with load test data.

ANCHOR AND SOCKET SYSTEMS

Anchors and sockets are three component systems consisting of: (1) steel tendons or reinforcing bars, (2) cement or resin grout, and (3) the rock mass itself, as shown in Figure 1-1. A tensile load applied to the tendon is transferred by means of shear stress in the grout to the rock mass. This basic framework covers rock bolts, anchors, and sockets, each of which has its own characteristics and uses as discussed below.

Rock bolts are structural elements used to preserve or improve the integrity of the rock mass in projects where the rock comprises the structure itself. Common applications include tunnels and rock slopes. Bolts are usually composed of a single reinforcing bar, either anchored at one end with the mid-section free, or completely grouted. Both mechanical and grout anchorages are common, and bolts are often prestressed to develop compression in the rock mass.

The function of rock anchors, in contrast to bolts, is to transfer tensile forces from an engineered structure to the rock mass. Applications include stays for re-

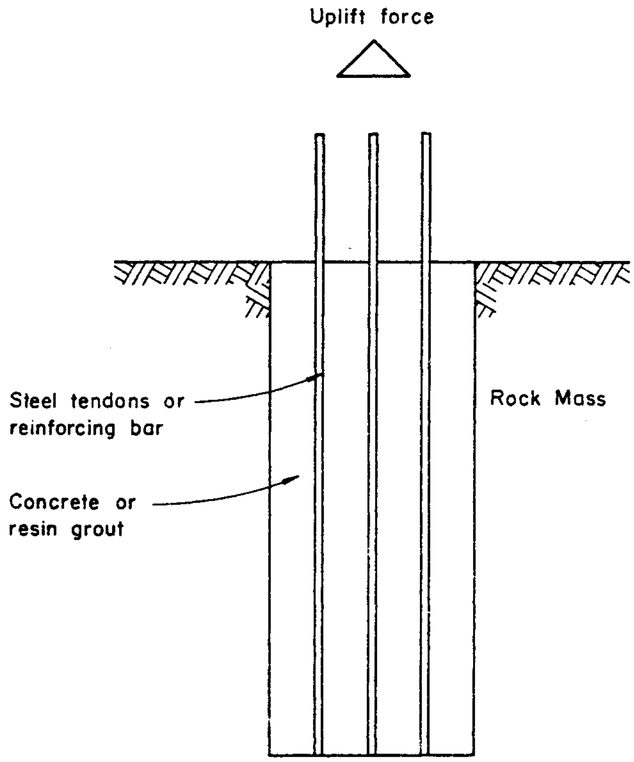

Figure 1-1. Anchor and Socket Geometry

taining walls and bulkheads, guy lines, temporary construction reactions, and rock slope stabilization. Rock anchors usually are composed of several reinforcing bars or a bundle of cables grouted into the rock. The forces imposed on anchors are often quite high, and can be either cyclic or static. The anchor also can be prestressed.

On a larger scale, rock socketed drilled shafts are used as foundations for large buildings and bridges. The function of sockets is primarily to increase capacity and reduce settlements. Sockets are usually in compression but are often subjected to repeated tensile forces from wind and other loads.

FAILURE MODES

Examination of rock anchorage systems reveals four locations where failure can occur:

1. steel

2. steel-grout interface
3. grout-rock interface
4. rock mass

At each location there is a different failure mode with its own behavior, failure criterion, and governing equations. Figure 1-2 illustrates the typical failure modes for each case; all are important because the entire system is only as strong as its weakest link.

Although all four failure modes are possible, some are more prevalent in specific field conditions than others. As a general rule, shallow anchors in heavily jointed rock masses will experience rock mass uplift before the grout-rock interface fails. Conversely, deep sockets fail at the grout-rock interface before rock mass failure can occur. The dividing line between these two modes is not clear because loosening of the rock mass upon uplift decreases the load transfer ability of the grout-rock interface.

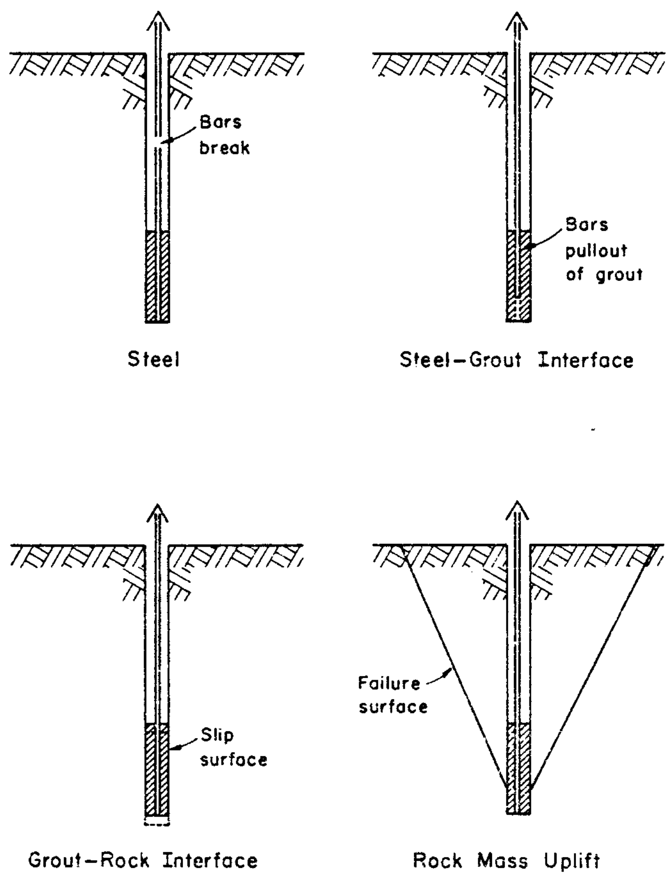

Figure 1-2. Failure Modes

Safety and economic considerations dictate that the design incorporate appropriate safety factors for all four modes into a balanced design. The primary focus of this study is failure at the grout-rock interface. However, a brief review of the other failure modes and their respective design principles are presented for clarity and completeness.

ROCK MASS PROPERTIES

A rock mass differs from the rock material because of discontinuities and other irregularities which can alter its performance. In the case of massive formations without significant jointing, the rock mass properties are nearly identical to the material properties. At the other end of the spectrum, a highly fractured rock mass may behave more like soil than rock.

The distinction between rock and soil is not precise. For purposes of this study, rock is defined as having a uniaxial compressive strength, q_u, of 1 MN/m^2 (145 psi) or higher. Highly porous materials such as some sandstones and limestones are excluded because of their crushability. The term rock mass is used to describe reasonably competent rock formations. These can be classified in Franklin, Broch, and Walton's (1) system (Figure 1-3) as low or better, or with a geomechanics classification (2) rock mass rating, RMR, of 20 or higher.

The properties of rock masses, unlike other system components, can not be specified to suit the situation; the designer must use the material available, modify it, or move the structure. Furthermore, the rock mass properties are not easily obtained although they are necessary for design purposes.

The methods available for estimating the rock mass elastic properties can be grouped into three categories: (1) in-situ testing, (2) empirical correlations, and (3) geomechanical models. In-situ testing ranges from seismic methods, in which a dynamic modulus is obtained, to borehole jacks and other down-the-hole devices, from which a localized in-situ modulus is measured, to field load tests, in which small-scale to full-scale behavior can be evaluated.

Empirical correlations use an index and field observations to establish an empirical relationship. Among the more popular indices are the rock quality designation, RQD, and rock mass rating, RMR. Deere, et al. (4) showed that the RQD approximately correlates with a reduction factor that can be used to estimate the rock mass modulus from the intact rock material modulus. Bieniawski (5) used the RMR, which is a rating based on six different parameters, to establish a tentative relation-

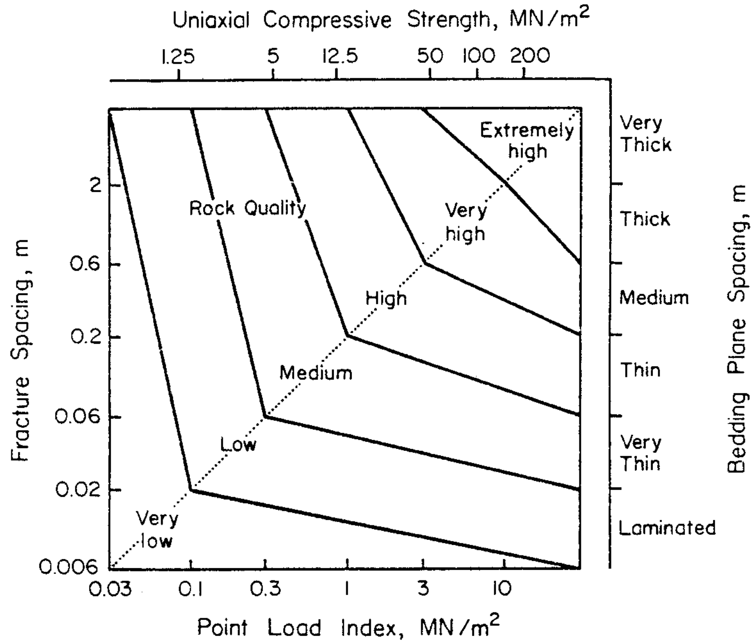

Figure 1-3. Franklin's Rock Quality Classification

Source: Reference (3), p. 51.

ship between the RMR and the in-situ modulus. Although the data base for both the RQD and RMR correlations are predominantly from tunnel or hydroelectric projects, they appear to be reasonable approximations for foundation evaluations.

The third approach is that of the geomechanical model, in which the rock material and discontinuity properties and geometry are used to calculate the equivalent rock mass properties. Both physical analogies (6, 7) and continuum mechanics analogies (8) have been used. This method is useful when the input parameters are defined adequately, but quantification of the discontinuity properties can be difficult.

DESIGN PRINCIPLES

Rock Mass Uplift

The capacity of anchors is limited by the ability of the rock mass to sustain tensile loads. Sound and continuous rock masses are usually capable of carrying the resulting stresses, and the grout-rock interface becomes the weak link. However, the presence of discontinuities within rock masses prevents the transfer of tensile stresses, especially near the surface where the overburden stress is small. Therefore, shallow anchors installed in highly fractured rock masses tend to fail by rock mass uplift.

Current design practice assumes that a failure surface in the shape of an inverted cone radiates upward from the base of the anchor. The anchor capacity is taken as the weight of material enclosed by the cone plus adjustments for material strength. The position of the apex and angle enclosed by the cone are obtained from empirical rules, such as those given in (9, 10, 11). Although this method is fairly popular, it has neither a theoretical basis nor a good background of experimental data. Actual design against rock mass uplift in highly fractured rock masses is most often based upon load testing at a specific site.

Steel

Steel design in anchors is both a structural problem of strength, and a practical problem of acceptable deformations. The concepts and specifications of steel and reinforced concrete design are directly applicable to the design of tendons and reinforcing bars in anchors.

Permissible tendon stresses are quoted in structural design codes as a percentage of yield strength for long term, short term, proof, and lock off loads. In the ACI Code 318-77 (12), these specifications are covered in Section 18.5. The acceptable deformation depends on how the anchor is being used and its influence on the primary structure. Both elastic and creep type of behavior must be considered in the design.

Steel-Grout Interface

The pullout resistance of bars and strands in concrete is a combination of bond, friction, and interlocking behavior. Similar principles apply for cement and other grouts. Tepfers (13) and Lutz and Gergely (14) showed that the resistance of plain steel tendons in concrete is a function of bond before displacement occurs, and friction afterwards. The resistance of deformed tendons is derived from an interlocking force and is limited by splitting of the concrete.

The concepts and specifications for development length of bars and strands in prestressed concrete beams are directly applicable to anchors. Development length is defined in the ACI code as "length of embedded reinforcement required to develop the design strength of reinforcement at a critical section." The development length varies with concrete strength, bar type, bar size, and steel yield strength.

Although several researchers (15, 16) have shown the distribution of stress along the bar to be highly nonlinear, a linear distribution is used in most codes and is assumed for design purposes. Specifications are given in the ACI Code 318-77, Sections 12.2.2 and 12.10, for bars and strands, respectively. Because of the influence of adjacent strands and spacers, the pullout capacity of groups of bars is reduced as per Section 12.4 in the ACI Code.

Grout-Rock Interface

Failure at the grout-rock interface is the most prevalent of the four modes. As with embedment of bars in concrete, the developed resistance is a function of material strength, bond, friction, and interlocking. The interaction of these factors is a complex problem and is examined in detail herein.

Although none of the four factors outlined above has a dominant influence on capacity, design methods are currently based on material strength. For design purposes, it is assumed that there is a uniform distribution of shear stress along the socket or anchor. The average unit shear resistance acting on the side wall is given as a reduction factor, α, times the uniaxial compressive strength of the rock or grout, whichever is weaker. Quantification of the reduction factor is achieved from correlations with q_u. Several authors have presented correlations of α and q_u for specific sites and socket geometries. A recent summary of these by Meigh (17) is given in Figure 1-4.

Use of the preceding methods gives a reasonable estimate of anchor and socket shear capacity under certain conditions. However, the capacity can be altered drastically by changing the character of the side wall. An irregular grout-rock interface allows for greater capacity, while a smooth interface decreases capacity and has the additional drawback of rapid post-peak strength loss. This roughness factor needs to be quantified.

Often design is based on allowable deformations rather than the ultimate capacity, but the preceding method gives no information on movements. Elastic movement analyses are fairly accurate, but are limited to a no slip condition which may be well below the socket capacity. Methods of calculating inelastic movements need to be refined and used.

SCOPE OF STUDY

Section 2 presents a comprehensive approach which governs the behavior of rock sockets and anchors. In the analysis, the behavior is assumed to progress through

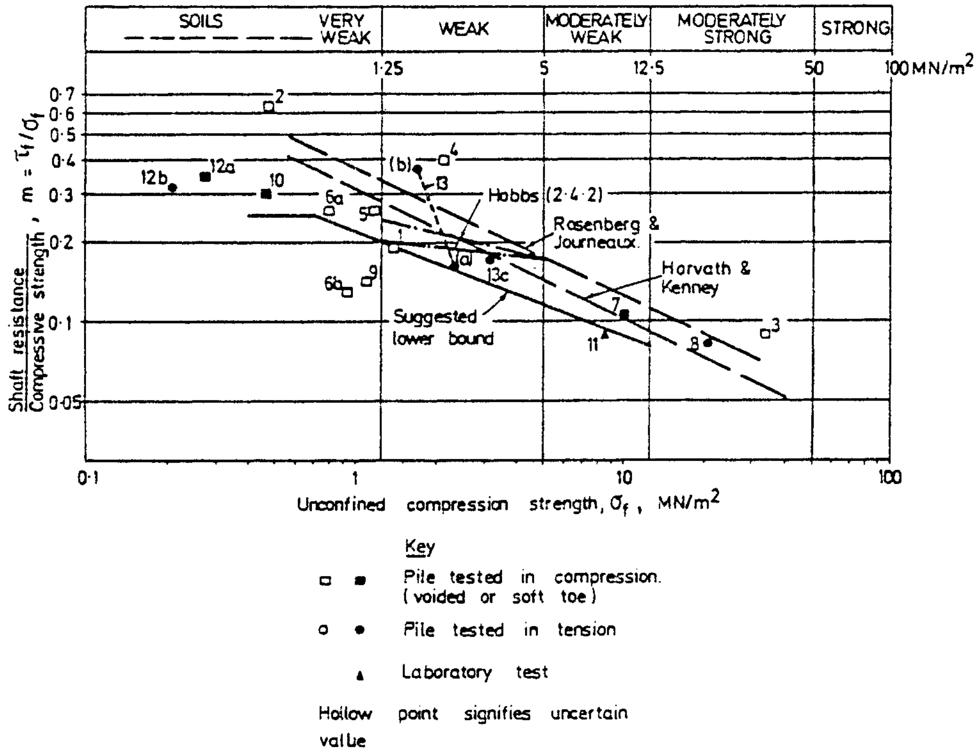

Figure 1-4. Reduction Factor vs. Uniaxial Compressive Strength

Source: Reference (17), p. 75.

stages of elastic, secondary, and residual conditions. At each stage, the behavior is described and relationships are given for the force-displacement behavior and capacity. The influence of factors such as strength, elasticity, roughness, and construction procedures are incorporated. The result is a complete analysis of socket behavior including capacity, displacements, and the influence of other factors.

Section 3 illustrates the use of the concepts and equations presented in Section 2. Load test data from a number of different locations are used to show how the equations are applied. In addition to showing the practicality of the method, Section 3 shows how variations in design parameters affect performance. As will be seen, socket behavior as modeled by the methods in Section 2 is sensitive to some factors, and insensitive to others. This is important in the actual design of sockets because the input parameters often are characterized by ranges, rather than precise values.

Section 4 investigates the rock mass uplift failure mode. A series of anchor load tests are used to illustrate the elastic and inelastic responses of anchor systems failing by uplift of the rock mass. The specific geometric and field conditions under which this mode prevails are discussed, and the transition into the grout-rock interface slip failure mode is described.

Section 5 concludes the work by presenting general comments on the method, its applications, and its limitations. Suggestions also are made for further research.

REFERENCES

1. Franklin, J. A., Broch, E., and Walton, G., "Logging the Mechanical Character of Rock," Transactions, Institute of Mining and Metallurgy, Vol. 81, Sect. A., 1972, pp. 43-51.

2. Bieniawski, Z. T., "Geomechanics Classification of Rock Masses and its Application in Tunneling," Proceedings, 3rd Congress of the International Society for Rock Mechanics, Vol. 2, Part A, Denver, 1974, pp. 27-32.

3. Goodman, R. E., Methods of Geological Engineering in Discontinuous Rocks, West Publishing Co., St. Paul, 1976, 427 p.

4. Deere, D. U., Hendron, A. J., Jr., Patton, F. D., and Cording, E. J., "Design of Surface and Near Surface Construction in Rock," Proceedings, 8th U.S. Symposium on Rock Mechanics, Minneapolis, 1967, pp. 237-302.

5. Bieniawski, Z. T., "Determining Rock Mass Deformability: Experience from Case Histories," International Journal of Rock Mechanics and Mining Sciences, Vol. 16, No. 5, Oct. 1978, pp. 237-247.

6. Goodman, R. E. and Duncan, J. M., "Finite Element Analysis of Slopes in Jointed Rock," Contract Report S-68-3, U.S. Army Engineer Waterways Experiment Station, Vicksburg, Feb. 1968, 276 p.

7. Kulhawy, F. H., "Geomechanical Model for Rock Foundation Settlement," Journal of the Geotechnical Engineering Division, ASCE, Vol. 104, No. GT2, Feb. 1978, pp. 211-227.

8. Gerrard, C. M., "Elastic Models of Rock Masses Having One, Two, and Three Sets of Joints," International Journal of Rock Mechanics and Mining Sciences, Vol. 19, No. 1, Feb. 1982, pp. 15-23.

9. Hobst, L., "Vizepitmenyek Kihorgonyzasa," Vizugi Koslemenyek, Vol. 4, 1965, pp. 475-515, (as referenced by Littlejohn, 11).

10. Saliman, R. and Schaefer, R., "Anchored Footings for Transmission Towers," Preprint 753, ASCE Annual Meeting, Pittsburgh, 1968, 28 p.

11. Littlejohn, G. S., "Rock Anchors - State of the Art, Part 1: Design," Ground Engineering, Vol. 8, No. 3, May 1975, pp. 25-32.

12. American Concrete Institute, Building Code Requirements for Reinforced Concrete (ACI 318-77), American Concrete Institute, Detroit, Mar. 1979, 103 p.

13. Tepfers, R., "A Theory of Bond Applied to Overlapped Tensile Reinforcement Splices for Deformed Bars," Publication No. 73:2, Chalmers University of Technology, Sweden, 1973, 328 p., (as referenced by Hanna, 18).

14. Lutz, L. and Gergely, P., "Mechanics of Bond and Slip of Deformed Bars in Concrete," Journal of the American Concrete Institute, Vol. 64, No. 11, Nov. 1967, pp. 711-721.

15. Hawkes, J. M. and Evans, R. H., "Bond Stresses in Reinforced Concrete Columns and Beams," Structural Engineer, Vol. 29, No. 12, Dec. 1951, pp. 323-327.

16. Phillips, S. H. E., "Factors Affecting the Design of Anchorages in Rock," Research Report R48/70, Cementation Research Ltd., London, 1970, (as referenced by Littlejohn, 11).

17. Meigh, A. C., "Design Parameters for Weak Rocks," Proceedings, 7th European Conference on Soil Mechanics and Foundation Engineering, Vol. 5, Brighton, 1979, pp. 59-79.

18. Hanna, T. H., Foundations in Tension, McGraw-Hill Book Co., New York, 1982, 573 p.

Section 2

ANALYSIS OF SOCKET BEHAVIOR

In this section, a comprehensive approach is developed for the behavior and design of sockets, focusing on the grout-rock interface. The transfer of stress from grout to rock can be based on either an elastic analysis, which assumes an intact or bonded interface, or an inelastic analysis, which assumes debonding and a relative displacement at the interface. The intact system is described by elastic solutions for settlement and for the distribution of the shear, axial, and normal stresses. The debonded system is described by inelastic equations based on the magnitude of displacement and character of the interface.

Initially, rock sockets are intact. As axial stress is applied to the foundation butt, it is distributed vertically and horizontally in accordance with the governing elastic equations. As the axial stress increases, the weaker zones and areas of stress concentration in the rock mass begin to fail. In this case, failure does not indicate a catastrophic loss of capacity; instead a discontinuity is created, leading to a shear displacement, and the foundation behavior becomes inelastic. With further increases in applied stress, the entire system progresses into inelastic behavior, termed secondary behavior herein. After a relatively large amount of displacement has occurred, the secondary behavior progresses into a residual state. The displacements necessary to attain the residual state are large, and are seldom achieved in sockets or anchors, except during load tests. However, the concept is a logical extension of secondary behavior and is useful for examining the limit state of behavior. Figure 2-1 illustrates the progression of behavior from elastic, to secondary, to residual, and shows how each is affected by roughness.

Roughness should be visualized as a variable with the extremes of interlocking and smooth. A precise definition of interlocking is difficult because it describes a behavioral tendency which is a function of several parameters, as opposed to being a simple geometric condition. Smooth represents the opposite extreme behavior. As seen in Figure 2-1, these extreme conditions bypass stages in the more general category of rough. The conditions necessary to attain these end points of

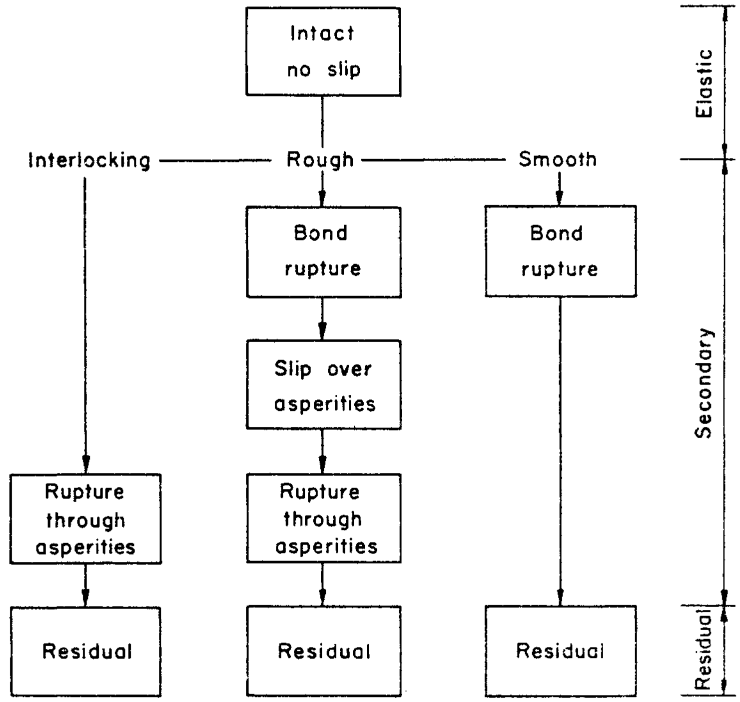

Figure 2-1. Behavioral Flow Chart

roughness, and the performance of each, are described in detail after the basic theory has been presented.

ELASTIC BEHAVIOR

Elastic solutions for load distribution and displacement of rock sockets can be obtained by analytical or numerical techniques. Since the solutions are elastic, there is no fundamental difference between a socket subjected to compression or extension loading, except for Poisson and tip effects. Solutions for combined side and tip-bearing sockets are not applicable because there is no similar tip effect during uplift loading.

Movement

Pells and Turner (1) presented the results of a finite element study of the settlement of side-resisting or shear sockets. They calculated the settlements from:

$$\rho = \left[\frac{P}{r\,E_m}\right] I_\rho \qquad (2\text{-}1)$$

in which ρ = settlement, P = applied axial load, r = foundation radius, E_m = Young's modulus for the rock mass, and I_ρ = influence factor.

The influence factor is a function of socket geometry and stiffness ratio, K_E, defined as $K_E = E_g/E_m$, in which E_g = Young's modulus for the grout. Values of I_ρ for a surface shear socket are presented in Figure 2-2. Pells and Turner noted that changes in Poisson's ratio had little effect on settlement. Embedment of the socket beneath the surface has the effect of reducing settlements; these reduction factors are given in Figure 2-3.

Stress Distribution

The analysis by Pells and Turner gives good results for settlement, but they did

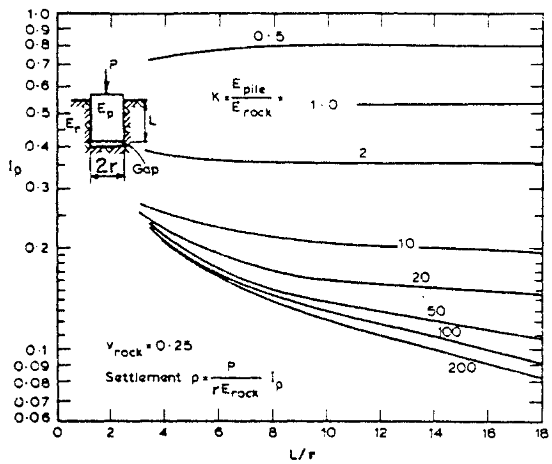

Figure 2-2. Elastic Settlement of a Shear Socket

Source: Reference (1), p. 482.

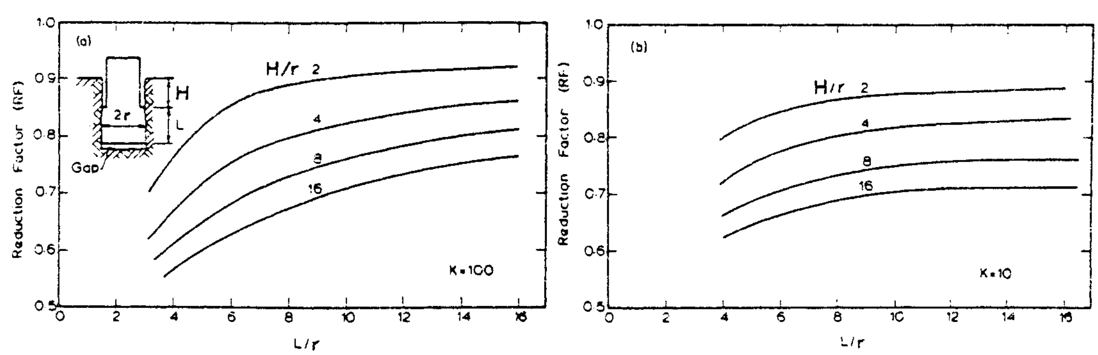

Figure 2-3. Embedment Reduction Factors

Source: Reference (1), p. 482.

not present the stress distributions for shear sockets. Therefore, a finite element study of shear sockets was conducted to determine the axial and shear stress distributions with depth for various socket geometries and material properties. Eight-noded quadrilateral elements were used to idealize the socket. Load transfer in tip resistance was eliminated by including a soft zone about one element thick beneath the socket tip. The meshes and other details of the analysis are presented in Appendix A.

The results of these finite element analyses are presented in Figure 2-4. As can be seen, the stress distribution is nonlinear, and is dependent on the relative stiffnesses of the grout and rock. When the stiffness ratio is unity, the system behaves as a homogeneous material subjected to a uniform load over a finite area. For this condition, Boussinesq's equations predict a large variation in stress along the socket, with the maximum in the upper two diameters and rapid decay with depth.

Relatively stiff rock masses or soft grout, having stiffness ratios, K_E, in the range of 0.1 to 1.0, behave in a similar manner, with higher concentrations of stress near the foundation butt for lower stiffness ratios. As the stiffness ratio approaches 10, signifying a stiff foundation in comparison to the rock, the shear stress distribution becomes nearly linear. Changes in Poisson's ratio have little effect on the stress distribution.

Short foundations with length to radius ratios of 2 or less have a relatively linear distribution of axial stress. Longer foundations with length to radius ratios of 4 or higher have more nonlinear axial stress distributions, with stress concentrated near the butt.

SECONDARY BEHAVIOR

Since the elastic solutions show a high concentration of shear stress near the foundation butt, it is likely that an initial failure zone will develop in that region. Failure in this case does not necessarily indicate a catastrophic loss of load-carrying capacity, but rather a change from elastic to inelastic behavior.

Localized failure is initiated with small displacements at the grout-rock interface. As long as part of the interface remains intact, relative displacements along the entire wall are restricted. Once a complete shear surface develops, significant displacements are possible, and secondary mechanisms take over.

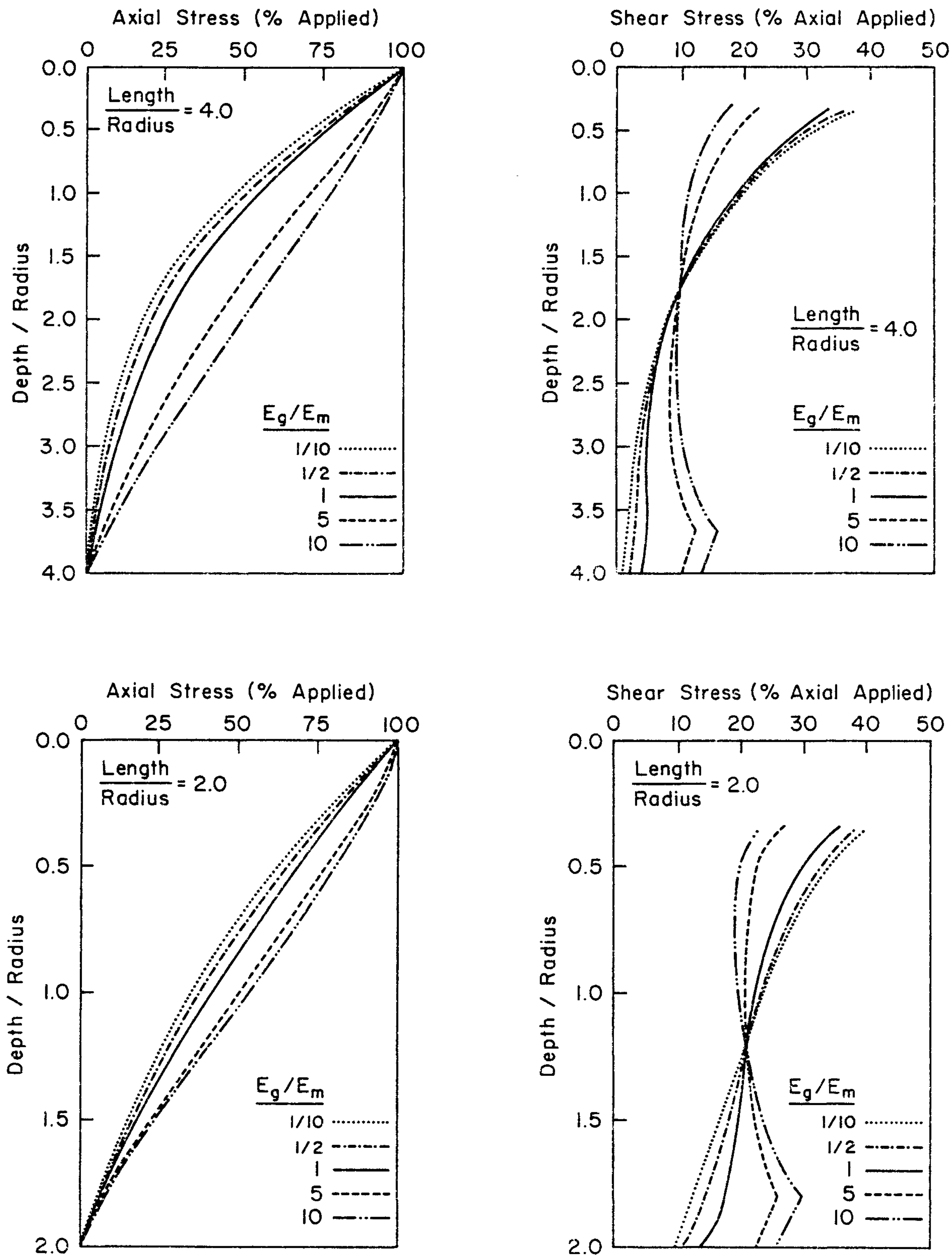

Figure 2-4. Stress Distribution with Depth

The failed interface, now free to move, can be modeled as a rock joint. Given that the joint is not perfectly smooth, a shear displacement causes a normal dilation which, in turn, creates a normal stress, as illustrated in Figure 2-5.

The asperities can be idealized as uniform triangles with identical initial dilation angles, i_o. Patton (2) showed that, at low normal stresses, the strength of this system is governed by sliding over the asperities and is given by:

$$\tau = \sigma_n \tan (i_o + \phi_b) \tag{2-2}$$

in which σ_n = normal stress and ϕ_b = base friction angle.

At high normal stresses, the system shear strength is governed by other parameters. Patton used a Mohr-Coulomb linear relationship of the form:

$$\tau = c_j + \sigma_n \tan \phi_b \tag{2-3}$$

in which c_j = cohesion intercept. Other strength envelopes can be used if they model the material more accurately.

Governing Equation

In Patton's tests, the teeth were spaced at regular intervals and had identical geometry. Therefore, the transition from the sliding mode of failure to the rock

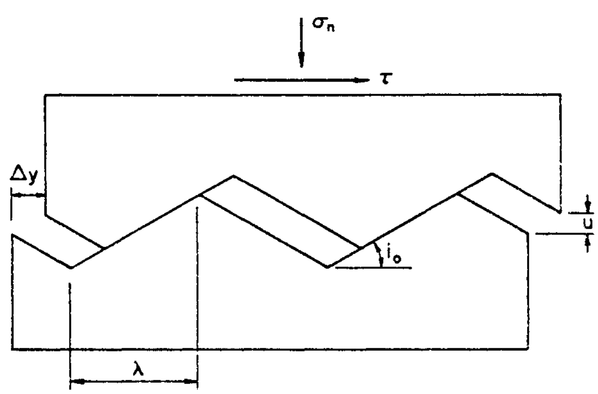

Figure 2-5. Joint Dilation

material strength mode occurred at a point. Natural rock joints and rock socket interfaces are characterized by irregular profiles with a distribution of asperity sizes and dilation angles. For these systems, the transition from the sliding mode to the rock strength mode is a progressive phenomenon, resulting in a curved, rather than a bilinear, failure envelope for the joint. Figure 2-6 illustrates Patton's bilinear model and shows how it relates to the more common curved joint failure envelope.

The shear strength envelopes illustrated in Figure 2-6 are for the peak shear strength of intact joints, each tested at a particular normal stress. Several forms of the joint shear strength formula have been proposed (3, 4, 5). Each of these can be used to model the peak shear strength, but they must be modified to accommodate progressive failure and post-peak behavior.

Dight and Chiu (6) modified Ladanyi and Archambault's equation (4) by incorporating a term for the degree of interlocking which decreases with displacement. Although they showed that this formulation can model the progressive failure of joints, careful analysis of some of the parameters reveals unrealistic trends with large deformations.

The equation proposed by Jaeger (5) can be modified to model progressive failure by including an area reduction factor, a_r. Jaeger's basic equation is illustrated in Figure 2-7, and is given by:

$$\tau = c_j \,[1 - \exp(-b\ \sigma_n/q_u)] + \sigma_n \tan \phi_b \qquad (2\text{-}4)$$

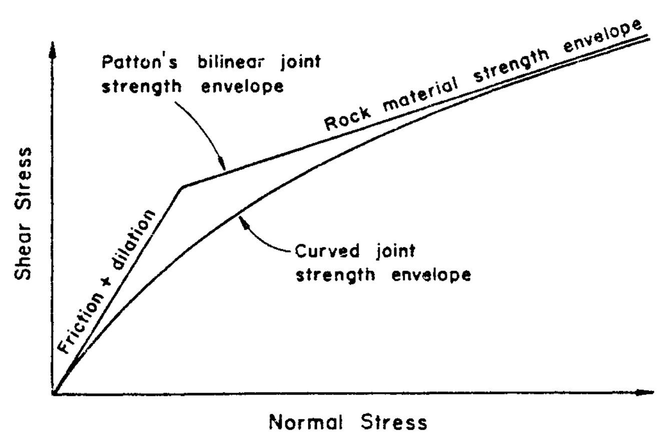

Figure 2-6. Rock Joint Strength Envelopes

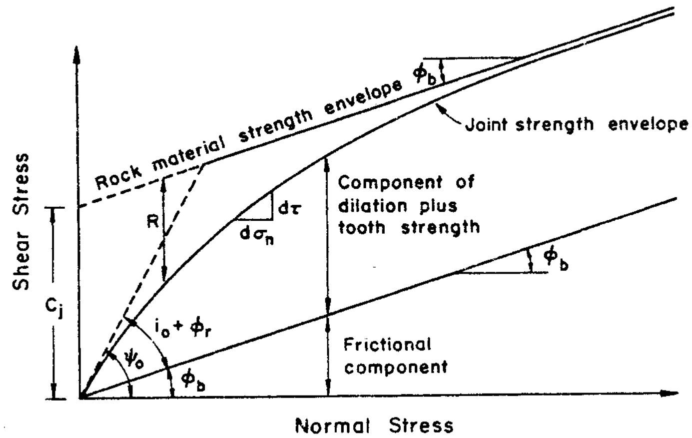

Figure 2-7. Jaeger's Rock Joint Strength Envelope

in which c_j = shear strength intercept and b = empirical constant. This equation assumes that the intact friction angle at high normal stresses is the same as the base angle for sliding. Although this is not strictly valid, the two angles are usually within a few degrees of each other, and the difference is commonly within experimental error.

Progressive Failure

The concept of progressive failure is incorporated into the analysis by introducing the area reduction ratio, a_r, defined as the ratio of available strength from the sum of dilatancy and tooth strength to the maximum for the intact joint. Equation 2-4 then is modified to:

$$\tau = c_j \ a_r \ [1 - \exp(-b \ \sigma_n/q_u)] + \sigma_n \tan \phi_b \tag{2-5}$$

At zero displacement, the joint is intact and a_r is equal to one. With large displacements, the asperities have all been sheared off, the rate of dilation is zero, and a_r decreases to zero. Between these extremes, a_r decreases as a function of displacement. An exponential decay function of the following form has been assumed:

$$a_r = \exp(-k_1 \ \Delta y) \tag{2-6}$$

in which k_1 = empirical constant to be evaluated experimentally and Δy = shear displacement.

By calculating a family of curves, each with a different value of a_r, the effect of varying this parameter can be assessed. As illustrated in Figure 2-8, envelopes with different a_r values are parallel at large normal stresses and converge to zero at low normal stress. The stress path for a typical rock joint subjected to shearing is superimposed on the curves to show how a_r changes during shearing. Initially, the stress path is parallel to the a_r = 1 curve, and degradation of the joint occurs by crossing the different envelopes until the residual condition is achieved at the base friction line.

To obtain a stress-strain curve or ultimate failure stress from Equation 2-5, an incremental method is used. Small increments of displacement are assumed and used to calculate the dilation and normal stress, from which the shear stress potential is determined. The constants, k_1, b, and c_j, and the normal stresses are calculated from the methods outlined in the following.

Cohesion Intercept, c_j

The intact strength envelope for a rock joint is the sum of 2 components: (1) friction and (2) a combination of dilation and strength of the asperities. These two components are shown in Figure 2-7 and are represented in Equation 2-4 by the tan

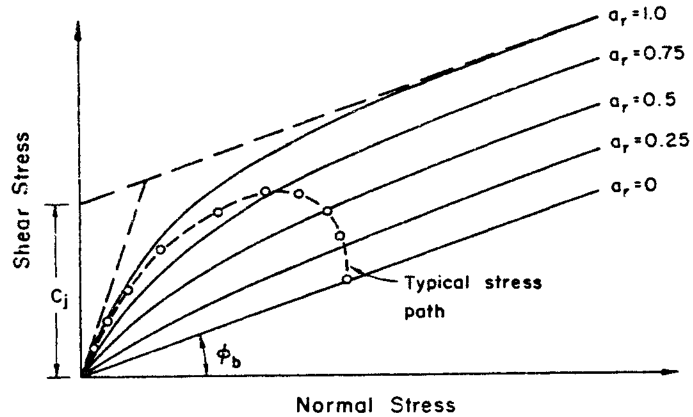

Figure 2-8. Family of Rock Joint Strength Envelopes for Different Values of the Area Reduction Ratio

ϕ_b and c_j terms, respectively.

The relative contributions of dilatancy and tooth strength to the c_j component of joint shear strength varies with normal stress. At high normal stress, tooth strength is the major component, while at low normal stress, dilations dominate. There is a transition between these extremes but, unfortunately, the data available are not adequate to separate the two components except at the end points. An estimate of c_j is obtained by back-calculating from q_u, using:

$$c_j = \frac{1}{2} q_u \left(\frac{1}{\cos \phi_b} - \tan \phi_b\right) \tag{2-7}$$

Calculation of b

The constant, b, can be obtained from either the initial slope of the stress path (τ vs. σ_n) or from graphical methods. The initial inclination of the shear strength envelope can be expressed either as an angle, ψ_o, or as a slope. The slope, or increase in τ with respect to σ_n, is obtained from the first derivative of Equation 2-4 evaluated at $\sigma_n = 0$:

$$\frac{d\tau}{d\sigma_n} = \frac{c_j\ b}{q_u} + \tan \phi_b \tag{2-8}$$

The initial angle is the sum of the initial dilation angle, i_o, base friction angle, ϕ_b, and a contribution from the strength of the teeth, ϕ_r (expressed as an equivalent angle). These angles are related to the initial slope by:

$$\frac{d\tau}{d\sigma_n} = \tan \psi_o = \tan (i_o + \phi_r + \phi_b) \tag{2-9}$$

By equating the two expressions for the slope and solving for b, an explicit equation is obtained:

$$b = q_u \left[\frac{\tan \psi_o - \tan \phi_b}{c_j}\right] \tag{2-10}$$

The constant b is calculated from this equation and from measurement of the initial slope of the τ vs. σ_n strength envelope, or by estimating the three constituent angles i_o, ϕ_r, and ϕ_b. A graphical procedure can also be used to evaluate b by solving Equation 2-4:

$$\ln R = -b \frac{\sigma_n}{q_u} + \ln c_j \tag{2-11}$$

in which $R = c_j + \sigma_n \tan \phi_b - \tau$ for a given point. By plotting ln R vs. σ_n/q_u for a series of tests on intact specimens, as illustrated in Figure 2-9, a line having a slope of -b results. For the limiting condition of $\psi_o = 90°$, b approaches ∞, and the joint shear strength envelope, Equation 2-4, simplifies to the Mohr-Coulomb strength envelope. At the other extreme of $\psi_o = \phi_b$, in which there is no dilatant or tooth strength component, b = 0 and Equation 2-4 simplifies to a line representing the base friction angle.

Calculation of k_1

The calculation of k_1 is made by solving Equation 2-5 for a_r, and substituting shear stress and normal stress test data for τ_p and σ_n:

$$a_r = \frac{\tau_p - \sigma_n \tan \phi_b}{c_j\,[1 - \exp(-b\,\sigma_n/q_u)]} \tag{2-12}$$

Plotting ln a_r vs. displacement for all the data points of a given test produces a straight line, the slope of which is $-k_1$.

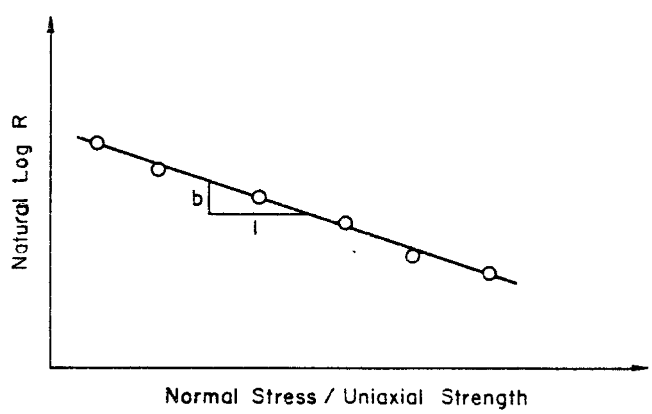

Figure 2-9. Determination of b

Normal Stress

In the direct shear test, the normal stress is constant and is derived from an applied load. However, in sockets the normal stress initially is close to zero and increases with increasing dilation. Therefore, the system is modeled correctly by a constant normal stiffness (CNS), rather than a constant normal stress.

By using elastic theory for expansion of an infinitely thick cylinder, the normal stress is estimated by:

$$\sigma_n = \frac{u}{r} \frac{E_m}{(1 + \nu_m)} \tag{2-13}$$

in which u = radial dilation and ν_m = Poisson's ratio of the rock mass. In terms of normal stiffness, k_n, the equation is:

$$k_n = \frac{\sigma_n}{u} = \frac{E_m}{(1 + \nu_m)} \frac{1}{r} \tag{2-14}$$

The effect of lateral expansion or contraction caused by Poisson's ratio of the foundation is included by adding the following term, derived from elastic theory by Kulhawy and Goodman (7):

$$\sigma_n = \left[\frac{\nu_g}{(1 - \nu_g) + (1 + \nu_m) E_g/E_m}\right] \sigma_y = Q \sigma_y \tag{2-15}$$

in which ν_g = Poisson's ratio for the grout, and σ_y = vertical stress in the foundation. The normal stresses from Equation 2-15 are subtracted from the dilation-generated normal stresses for uplift loading.

Dilations

The preceding equations use dilation as an input parameter to obtain the normal stress. Unfortunately, this aspect of rock joint and rock socket behavior has received little attention from researchers.

At small stresses, the rate of dilation, $\dot{u}$, is the same as tan i_o. However, as the normal stress approaches the transition stress, σ_T, dilations are suppressed, and the rate of dilation approaches zero. Ladanyi and Archambault (4) showed that the following equation based on i_o and σ_T gives a reasonable estimate of the rate of dilation:

$$\dot{u} = \left(1 - \frac{\sigma_n}{\eta \, \sigma_T}\right)^{k_2} \tan i_o \qquad (2\text{-}16)$$

in which k_2 is an empirical constant determined by Dight and Chiu (6) to be equal 3.0, and η is the degree of interlocking which is defined later.

The actual dilations are obtained by integrating $\dot{u}$ with displacement. However, since σ_n and η are functions of u, the solution of the resulting differential equation is a difficult task. A more practical approach is to assume small increments of displacement, update the normal stress and rate of dilation, and sum the total dilation incrementally.

Transition Stress

The transition stress is the confining stress at which the rock changes from brittle to ductile behavior. In connection with shear strength, the transition stress is the confining stress at which the shear strength of a fracture is greater than the rock material strength. Therefore, new fractures would develop in preference to sliding along pre-existing fractures.

Mogi (8) observed that the transition stress is a function of the major and minor principal stresses, σ_1 and σ_3, respectively. In his analysis, the transition stress is the confining stress at failure which satisfies the relationship:

$$\sigma_1 - \sigma_3 = 3.4 \, \sigma_3 \qquad (2\text{-}17)$$

Byerlee (9) developed a similar equation, given by:

$$\sigma_1 - \sigma_3 = 2.31 \, \tau \qquad (2\text{-}18)$$

Goodman (10) proposed that the transition stress can be estimated by the uniaxial compressive strength of the rock, if better data are unavailable:

$$\sigma_T = q_u \qquad (2\text{-}19)$$

The choice of which criterion to use depends on the rock type and data available.

Table 2-1

BRITTLE TO DUCTILE TRANSITION STRESSES FOR ROCKS AT ROOM TEMPERATURE

Rock Type	Gage Stress (MN/m^2)	(psi)
Rock salt	0	0
Chalk	<10	<1500
Compaction shale	0-20	0-3000
Limestone	20-100	3000-15,000
Sandstone	>100	>15,000
Granite	≫100	≫15,000

Source: Reference (<u>11</u>), p. 69.

The rock type is especially important because the transition stress varies greatly with mineralogy. Table 2-1 shows the typical variation of σ_T with rock type. This table is not intended to be a substitute for testing; instead it is an illustration of the range in σ_T and its dependence on mineralogy.

Roughness Quantification

Determination of the initial dilation angle is not a simple procedure because socket wall asperities are highly irregular. For this reason, statistical methods are useful in describing the wall profile.

Krahn and Morgenstern (12) found that two statistical parameters, the root-mean-square of the asperity height, RMS, and root-mean-square of the asperity angle, z_2, give a good description of roughness. For an irregular profile as illustrated in Figure 2-10, these are defined as:

$$RMS = \sqrt{\frac{1}{N} \int_{x=0}^{N} h^2 \, dx} \qquad (2\text{-}20)$$

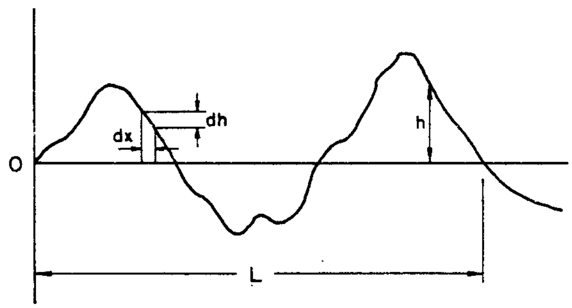

Figure 2-10. Definition of Variables for an Irregular Profile

Source: Reference (12), p. 130.

and $$z_2 = \sqrt{\frac{1}{L}\int_{x=0}^{L} \left(\frac{dh}{dx}\right)^2 dx} \tag{2-21}$$

in which N = number of measurements and L = length of the profile analyzed. When discrete measurements are used, instead of a continuous profile, the integrals become summations, and RMS and z_2 represent the standard deviation of the asperity height, SD_h, and standard deviation of the asperity angle, SD_i, respectively.

Based on SD_h and SD_i, Dight and Chiu (6) showed that a triangular profile (Figure 2-11) can be used to idealize the irregular profile. The initial dilation angle, i_o, and asperity height, h_m, are given by:

$$i_o = i_a + k_3 SD_i \tag{2-22}$$

and $$h_m = h_a + k_4 SD_h \tag{2-23}$$

in which i_a = average angle across the entire profile, h_a = average asperity height, k_3 = empirical constant equal to 1.0, and k_4 = empirical constant equal to 2.0.

Based on i_o and h_m, the half wavelength of the asperities, λ, is defined as:

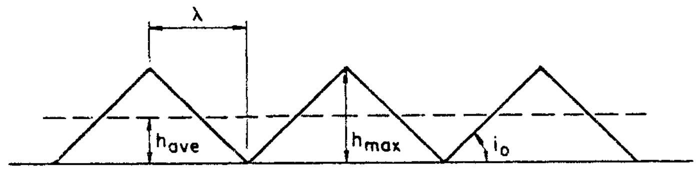

Figure 2-11. Definition of Variables for a Regular Profile

Source: Reference (6), p. 377.

$$\lambda = \frac{h_m}{\tan i_o} \tag{2-24}$$

and the degree of interlocking, η, is defined as:

$$\eta = (1 - \frac{\Delta y}{\lambda}) \tag{2-25}$$

in which Δy = shear displacement. The degree of interlocking is used to estimate the true contact area of a joint as shearing progresses.

Two methods are currently available to estimate the asperity angle standard deviation: direct measurement and standard correlations. Direct measurement techniques use a digitized surface profile, obtained from analysis of a photograph of the interface, to calculate the relevant statistical properties. The method of standard correlations is based on relationships obtained from the statistical analysis of Barton's Joint Roughness Coefficient, JRC, profiles (3) presented in Figure 2-12. Williams (14) presented the correlation between JRC and SD_i presented in Figure 2-13.

RESIDUAL BEHAVIOR

Excessive displacements along the grout-rock interface cause the system to revert into a residual state, characterized by no further changes in the load transfer behavior. A true residual state is achieved only after very large displacements have occurred, but the basic mechanisms begin to become established at lesser displacements. Also the concept is useful for describing the degradation of secondary behavior into the limiting condition.

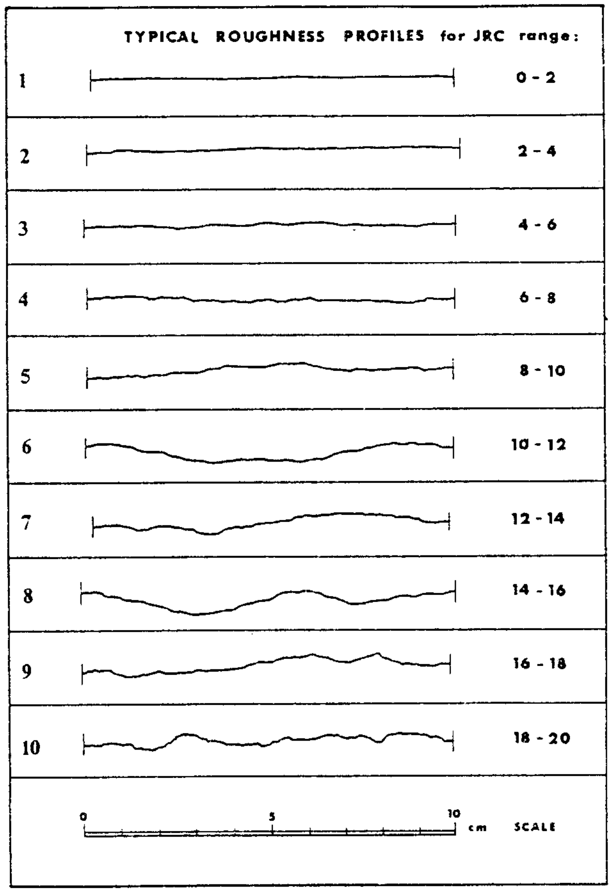

Figure 2-12. Joint Roughness Profiles

Source: Reference (13), p. 345.

The basic equations governing secondary behavior lose their validity after the asperities have sheared off. The capacity for this condition is a function only of the residual normal stress and base friction angle, and is given by:

$$\tau = \sigma_n \tan \phi_b \qquad (2\text{-}26)$$

The base friction angle, as it is used in this study, describes the friction between flat, horizontal rock surfaces, and is a function only of the composition and geometry of the rock mineral grains. Small surface irregularities along the fractures increase the apparent friction angle, ϕ_a, to a value above ϕ_b. As the irregularities are polished, ϕ_a reduces to ϕ_b and the transition is made from secondary

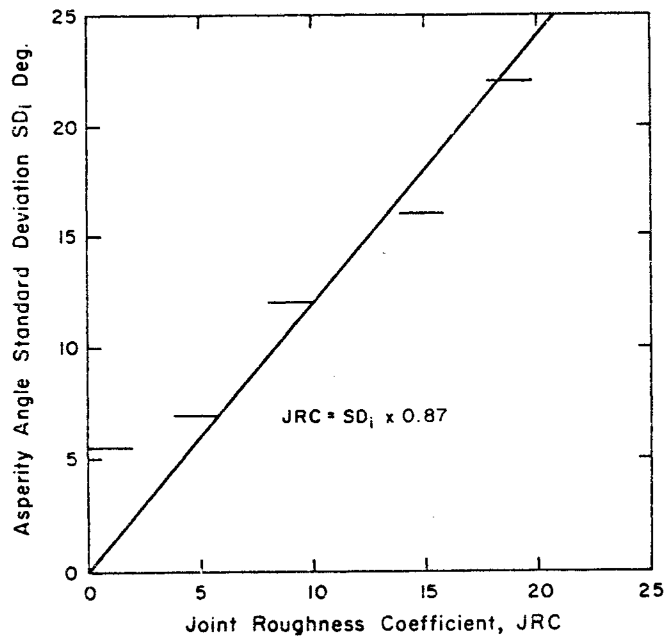

Figure 2-13. Correlation of Joint Roughness Coefficient with Dilation Angle

Source: Reference (14), p. 89.

to residual behavior. Table 2-2 gives typical values of ϕ_b for various rock types.

Information on the actual dilations and normal stresses for the residual condition is scarce, thereby preventing verifiable conclusions from being made. However, the results of CNS direct shear tests, and full-scale load tests conducted by Dight and Chiu (6) and Williams (14), allow the following generalizations to be made.

Figure 2-14 from a CNS direct shear test by Williams shows the typical trends of dilation, normal stress, and shear stress with shear displacement. Note that the dilation and normal stress each peak at a displacement of 10 mm while the shear stress peaks at 5 mm. If the peak shear stress represents failure of the teeth, then this indicates that dilations can be generated by mechanisms other than sliding across the asperities.

A possible model for this behavior is that of rotational dilation, described by Nascimento and Teixeira (16). Rotation of broken asperities and other debris along the shear surface causes dilation and normal stress as shown in Figure 2-15.

Table 2-2

BASE FRICTION ANGLES

Material	ϕ residual (degrees)	Material	ϕ residual (degrees)
Amphibolite (dry)	32	Melbourne Mudstone	25-35
Attapulgite	30	Montmorillonite	4-10
Basalt (dry)	35-38	Muscovite	17-24
Basalt (wet)	31-36	Quartz (crushed)	35
Calcite (crushed)	30	Quartz Monzonite	32
Chalk (wet)	30	Sandstone	25-34
Conglomerate	35	Sandstone (clean diamond cut)	36
Dolostone (dry)	31-37	Sandstone (bentonite coated, diamond cut)	32
Dolostone (wet)	27-35	Shale (wet)	27
Feldspar (crushed)	35	Siltstone (dry)	31-33
Gneiss (schistose)	23-29	Siltstone (wet)	27-31
Granite	29-35	Slate (dry)	25-30
Kaolinite	15		
Limestone	33-37		

Source: Reference (15), p. 95.

The second point to note from Figure 2-14 is that the shear stress drops off after attaining a maximum and eventually achieves a stable residual condition, while the dilation and normal stress are nearly constant, or decrease very slowly, after reaching their maxima. Therefore, the decrease in shear capacity is the result of smoothing of the remaining surface roughness, rather than a decrease in normal stress.

At this time, insufficient data are available to obtain quantitative relationships

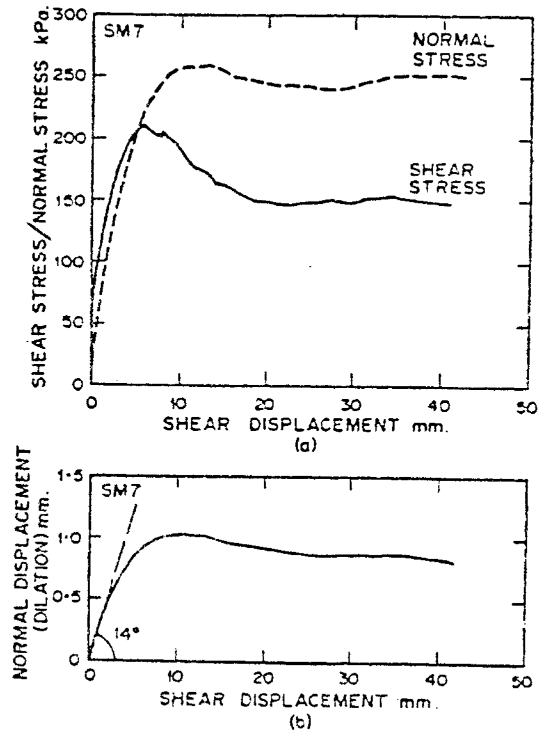

Figure 2-14. Typical Behavior for a 'Rough' Socket

Source: Reference (14), p. 90.

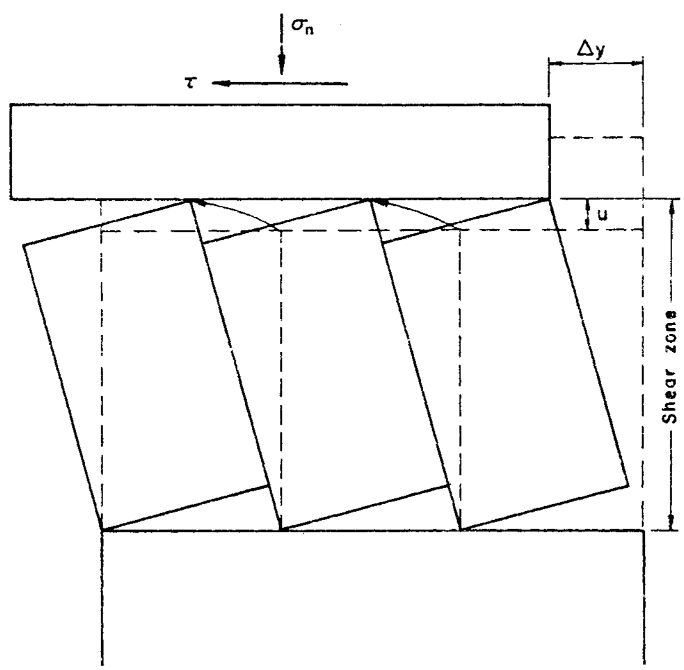

Figure 2-15. Rotational Dilation

for the post-peak loss in shear capacity. However, looking at the results of direct shear tests on rock joints, the following points can be made:

1. The normal stress increases with increasing stiffness, although the dilation decreases (14).
2. The ratio of residual to peak shear stress approaches unity as the normal stress increases. Presumably, there is a limiting value of σ_n equal to σ_T, at which the shear stress does not decrease after achieving its maximum value (17).
3. Sockets with relatively rough side walls show less post-peak shear stress loss than smoother interfaces. This last point introduces the next sub-section which examines the extremes of roughness and their corresponding behavior.

INTERLOCKING CONDITION

Definition

The shear strength equation developed by Ladanyi and Archambault (4) assumes there is a pre-existing shear surface along which displacement occurs. This condition is not always met because a bond, or exceptionally steep asperities, effectively can prevent the slip surface from developing.

Interlocking behavior is defined as the extreme condition of roughness in which shearing occurs through the asperities in preference to slip over them. The conditions in which this would happen are outlined below.

Conditions Necessary for Interlocking

Without a grout-rock bond, asperities protruding normal to the interface would effectively interlock the system. When the sum of the dilation and friction angles is 90° or more, a similar condition exists. As seen in Table 2-2, ϕ_b ranges from about 25° to 40°, and therefore the interlocking condition would be achieved for i_o = 50° to 65°, regardless of rock strength.

If an initial normal stress acts on the system, the change from first slip to complete interlocking behavior is a function of both the rock strength and the strength from dilation plus friction. This condition is evaluated by comparing the interlocked strength of the interface, which is a function of the material strength, with the friction plus dilation strength of the interface. The system is effectively interlocked when the interface slip shear strength (Equation 2-27) exceeds the material strength. In this case a Mohr-Coulomb strength envelope is assumed (Equation 2-28):

$$\tau = \sigma_n \tan (i_o + \phi_b) \tag{2-27}$$

$$\tau = c_j + \sigma_n \tan \phi_b \tag{2-28}$$

For conditions in which an initial bond, B, exists at the interface, Equation 2-27 is modified to:

$$\tau = \frac{B}{\cos i_o - \sin i_o \tan \phi_b} + \sigma_n \tan (i_o + \phi_b) \tag{2-29}$$

The preceding equations assume a regular triangular profile, which is only a mathematical idealization. The functional dilation angle for actual interfaces must be obtained by statistical methods, or be correlated with the JRC as outlined previously.

Field evidence for the transition from rough to interlocking behavior is scarce. Few researchers, and fewer contractors, take the time to describe the side wall roughness before testing. Therefore, force-displacement curves are available, but the socket wall roughness must be inferred from drilling procedures.

Results of a study on small diameter model shafts by Horvath and Kenney (18) give insight into the conditions necessary for interlocking and are shown in Figure 2-16. This figure illustrates how side friction varies with side wall shape (roughness). Although the exact positions of the points and line are open to interpretation, the general trend shows an increase in shear resistance with roughness. Furthermore, a maximum shear resistance of $q_u/2$ is achieved between the 'rough' and 'shaped' roughnesses, at which point further increases in roughness have little influence on shear capacity. The maximization represents the interlocking condition.

Interlocking Behavior

The typical load-displacement behavior of an interlocked socket is presented in Figure 2-17. The first stage of elastic response is terminated when a shear surface propagates downward near the grout-rock interface. As displacements along the interface increase, dilations also increase from a combination of rotating, wedging, and sliding. A gradual softening occurs as dilations are maximized and roughnesses are worn away. The post-peak strength loss experienced in some rough sockets does not occur for this condition.

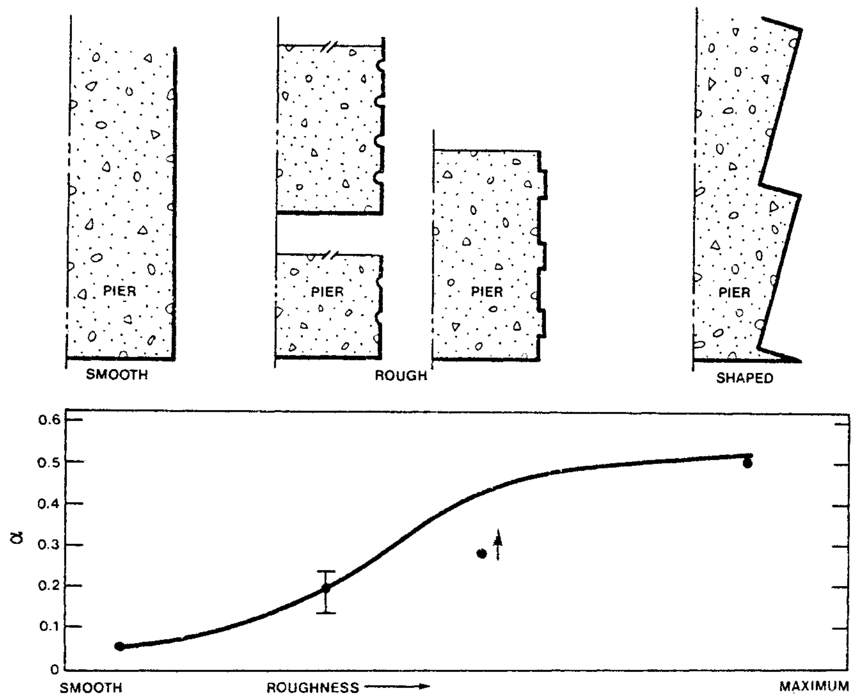

Figure 2-16. Shaft Resistance vs. Roughness of Socket Wall

Source: Reference (18), p. 199.

The capacity of interlocking sockets is a function only of the material properties and the normal stress acting on the system; the effects of the initial roughness and dilation angle have already been maximized. Capacity is governed by the same mechanisms and equations as for the residual condition, and is given by:

$$\tau = \sigma_n \tan \phi_b \tag{2-30}$$

Since the residual friction angle is constant for a given rock material, the capacity is a function only of the normal stress, which is generated from dilations at the interface and the initial horizontal stress. No experimental data have been found in the literature on the actual dilations and normal stresses experienced in this type of system. However, from a combination of theoretical considerations and analysis of load-displacement curves, the following points can be made:

1. The capacity of the system should be limited by σ_T, above which greater dila-

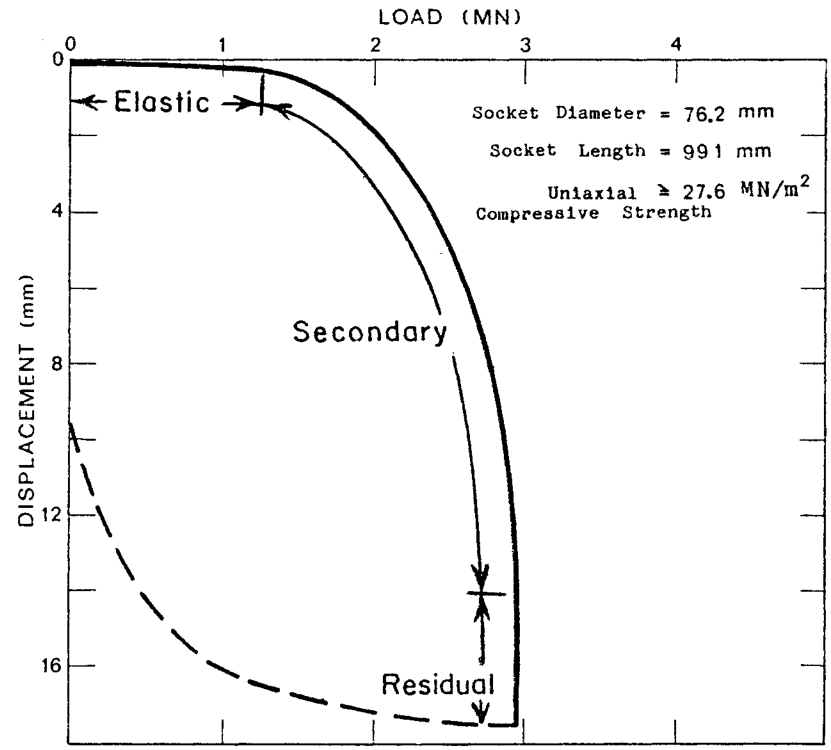

Figure 2-17. Typical Behavior for the 'Interlocked' Condition

Source: Reference (19), p. 351.

tions would be suppressed in favor of development of a new failure surface. Assuming that dilations are large enough to generate σ_T, and using q_u as an estimate of σ_T, Equation 2-30 becomes:

$$\tau = q_u \tan \phi_b \tag{2-31}$$

For typical ranges in ϕ of 25° to 40°, τ ranges from 0.47 q_u to 0.84 q_u. These values correspond well to the maximum values of α measured in the field, as shown in Figure 1-4.

2. For normal stresses less than the transition stress, the capacity is given by:

$$\tau = \frac{u}{r} \frac{E_m}{(1 + \nu_m)} \tan \phi_b \tag{2-32}$$

which assumes elastic side wall response and initial radial stress of zero.

3. The dilation necessary to achieve the transition stress probably does not vary much with rock strength. Using q_u as an estimate of σ_T, the necessary dilation is given by:

$$u_c = \frac{q_u}{k_n} = \frac{q_u}{E_m} (1 + \nu_m)\ r \tag{2-33}$$

   Since the ratio q_u/E_m is relatively constant for a given rock type, u_c is also relatively constant.

4. The dilations actually achieved in rough sockets are directly related to the irregularity of the failure surface which develops. Experimental data on the character of the failure surface for different rock types and loading conditions are necessary to continue the analysis in this direction.

5. Stronger and more competent rock and rock masses may develop relatively smooth failure surfaces, as opposed to weaker rocks which probably have a more irregular fracture surface. This could account for the relatively low α values characteristic of higher strength rocks.

SMOOTH CONDITION

Just as the interlocking condition represents one extreme of roughness, smooth represents the opposite extreme. The smooth condition is characterized by having no asperities at the grout-rock interface; therefore dilations are not possible, and there is no secondary behavior. A truly smooth condition is rarely, if ever, achieved because drilling procedures leave small irregularities along the side wall. However, many systems tend toward this condition, and the concept is useful for describing smooth behavior as a limiting condition.

The capacity of smooth systems is dependent only on the grout-rock bond strength. Breakage of the bond is often a sudden event accompanied by a large drop in capacity. Figure 2-18 shows the typical behavior of a smooth socket. For test B1, with roughness class R1, a rapid rise in shear stress occurs over the elastic range. This is followed by an equally rapid strength loss to a residual condition, sustaining less than 50 percent of the maximum load. This is an undesirable situation because there is no warning of failure, and there is a substantial reduction in capacity.

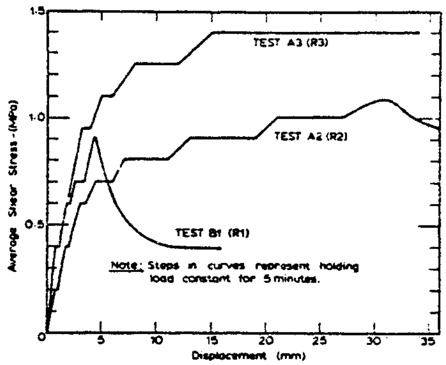

Roughness Classification

Roughness Class	Description
R1	Straight, smooth sided socket, grooves or indentations less than 1.00mm deep
R2	Grooves of depth 1-4mm, width greater than 2mm, at spacing 50mm to 200mm
R3	Grooves of depth 4-10mm, width greater than 5mm, at spacing 50mm to 200mm
R4	Grooves or undulations of depth > 10mm, width > 10mm at spacing 50mm to 200mm

Figure 2-18. Behavior of a 'Smooth' Rock Socket

Source: Reference (20), pp. 294 and 300.

For engineering purposes, there are two practical questions to address in reference to smooth sockets: (1) how much roughness is necessary to prevent this type of behavior, and (2) under what field conditions are problems likely to occur?

Referring to Figure 2-18, it can be seen that test B1 behaves in a brittle manner, with significant post-peak strength loss, in contrast to the more plastic behavior of test A2, which peaks gradually and maintains a high capacity. The roughness classifications for tests B1 and A2 are given as 1 mm and 1 to 4 mm, respectively, indicating that, for these tests, the transition from brittle (smooth) to plastic (rough) behavior occurs between 1 mm and 4 mm. Pells, Rowe, and Turner (20) concluded that "a roughness equivalent to 2 to 3 mm is sufficient to prevent 'brittle' behavior." Although these results were summarized from only one series of tests, they show that a relatively small roughness is enough to prevent the brittle behavior characteristic of smooth sockets.

The character of the rock mass, in particular the rock strength and discontinuities, indirectly influences the roughness. Joints and bedding planes cause irregularities in the socket side wall, thereby creating an effective roughness in an otherwise smooth hole. Weak rock material has a similar beneficial effect on roughness because of increased overbreak. These two notes on roughness partially explain why the unit side resistance reduction factor, α, decreases with increasing rock strength.

SUMMARY

The preceding sections describe in detail the behavior of the grout-rock interface of rock anchors and sockets. The behavior is seen to progress through three separate stages from elastic, to secondary, to residual. The conditions necessary to achieve each stage, and the equations governing capacity and behavior are outlined.

Elastic methods, primarily finite element numerical studies, are used to describe the settlements and stress distributions for the intact stage. Secondary behavior is modeled as a dilatant rock joint confined by a normal stiffness. Failure of the joint comes from a combination of slip over the asperities and rupture through the teeth. This general framework covers the entire range of roughness which varies from smooth to interlocking. The residual condition is described as the complete degradation of secondary behavior in which the asperities have all failed, and an equilibrium condition is achieved.

Verification of these principles and equations, and an illustration of their practical application, is presented in Section 3.

REFERENCES

1. Pells, P. J. N. and Turner, R. M., "Elastic Solutions for the Design and Analysis of Rock Socketed Piles," Canadian Geotechnical Journal, Vol. 16, No. 3, Aug. 1979, pp. 481-487.

2. Patton, F. D., "Multiple Modes of Shear Failure in Rock," Proceedings, 1st Congress of the International Society for Rock Mechanics, Vol. 1, Lisbon, 1966, pp. 509-513.

3. Barton, N. and Choubey, B., "The Shear Strength of Rock Joints in Theory and Practice," Rock Mechanics, Vol. 10, Nos. 1 & 2, Dec. 1977, pp. 1-54.

4. Ladanyi, B. and Archambault, G., "Simulation of Shear Behavior of a Jointed Rock Mass," Proceedings, 11th U.S. Symposium on Rock Mechanics, Berkeley, 1969, pp. 105-125.

5. Jaeger, J. C., "Friction of Rocks and the Stability of Rock Slopes," Geotechnique, Vol. 21, No. 2, June 1971, pp. 97-134.

6. Dight, P. M. and Chiu, H. K., "Prediction of Shear Behavior of Joints Using Profiles," International Journal of Rock Mechanics and Mining Sciences, Vol. 18, No. 5, Oct. 1981, pp. 369-386.

7. Kulhawy, F. H. and Goodman, R. E., "Design of Foundations on Discontinuous Rock," Proceedings, International Conference on Structural Foundations on Rock, Vol. 1, Sydney, 1980, pp. 209-220.

8. Mogi, K., "Pressure Dependence of Rock Strength and Transition from Brittle Fracture to Ductile Flow," Bulletin, Earthquake Research Institute, Vol. 44, Tokyo University, 1966, pp. 215-232, (as referenced by Dight and Chiu, 6).

9. Byerlee, J. D., "Brittle-Ductile Transition in Rocks," Journal of Geophysical Research, Vol. 73, No. 14, July 1968, pp. 4741-4750.

10. Goodman, R. E., Methods of Geological Engineering in Discontinuous Rocks, West Publishing Co., St. Paul, 1976, 472 p.

11. Goodman, R. E., Introduction to Rock Mechanics, John Wiley & Sons, New York, 1980, 478 p.

12. Krahn, J. and Morgenstern, N. R., "The Ultimate Frictional Resistance of Rock Discontinuities," International Journal of Rock Mechanics and Mining Sciences, Vol. 16, No. 2, Apr. 1979, pp. 127-133.

13. Barton, N., Coordinator for ISRM, Commission on Standardization of Laboratory and Field Tests, "Suggested Methods for the Quantitative Description of Discontinuities in Rock Masses," International Journal of Rock Mechanics and Mining Sciences, Vol. 15, No. 6, Dec. 1978, pp. 319-368.

14. Williams, A. F., "Principles of Side Resistance Development in Rock Socketed Piles," Proceedings, 3rd Australia-New Zealand Conference on Geomechanics, Vol. 1, Wellington, 1980, pp. 87-94.

15. Putnam, J. B., "Analysis and Design of Foundations on Discontinuous Rock," M. S. Thesis, Syracuse University, May 1981, 204 p.

16. Nascimento, U. and Teixeira, H., "Mechanisms of Internal Friction in Soils and Rocks," Proceedings, ISRM Symposium on Rock Fracture, Nancy, 1971, Paper 2-3, (as referenced by Goodman, 10).

17. Goodman, R. E., "The Mechanical Properties of Joints," Proceedings, 3rd Congress of the International Society for Rock Mechanics, Vol. 1, Part A, Denver, 1974, pp. 127-140.

18. Horvath, R. G. and Kenney, T. C., "Shaft Resistance of Rock-Socketed Drilled Piers," Proceedings, Symposium on Deep Foundations, ASCE, Atlanta, 1979, pp. 182-214.

19. Horvath, R. G., Trow, W. A., and Kenney, T. C., "Results of Tests to Determine Shaft Resistance of Rock-Socketed Drilled Piers," Proceedings, International Conference on Structural Foundations on Rock, Vol. 1, Sydney, 1980, pp. 349-361.

20. Pells, P. J. N., Rowe, R. K., and Turner, R. M., "An Experimental Investigation into Side Shear for Socketed Piles in Sandstone," Proceedings, International Conference on Structural Foundations on Rock, Vol. 1, Sydney, 1980, pp. 291-302.

Section 3

VERIFICATION AND APPLICATIONS

The mechanics of grout-rock interface behavior were examined in Section 2 for rock anchors and sockets. Equations also were presented to evaluate the behavior and capacity of these systems. This section focuses on verification and application of these equations. First, the equations are evaluated to determine how well they model rock anchor and socket behavior. Second, a data base of empirical constants for these equations is developed from back-calculation of load test data. Third, examples are presented which illustrate the use of the proposed method for predicting the behavior and capacity. Finally, the sensitivity of the proposed method to variations in the input parameters is examined.

DIRECT SHEAR TEST ANALYSIS

Equation 2-5, the basic shear strength equation, requires the evaluation of three empirical constants: k_1, k_2, and b. The constant normal stiffness (CNS) direct shear test is a useful tool for obtaining these parameters, because the normal stiffness, displacement, and shear stress can be controlled, and the dilation and normal stresses can be measured accurately.

A series of seven CNS direct shear tests on mudstone-concrete interfaces, conducted by Dight and Chiu (1), provides a good initial data base. The basic geometry, material properties, and test conditions are presented in Table 3-1. The calculations described below were performed on the test results, all of which showed similar trends. Test SM7 has been chosen as a typical example for illustrative purposes. Figures for the remaining tests are given in Appendix B.

Calculation of Constants

A first estimate of the constant, b, was obtained from the initial inclination of the stress path, ψ_0, as shown in Figure 3-1 and Equation 2-10. The initial inclination of the stress path is subjective and the resulting calculation of b can be variable. For this reason, the calculation of b by this method is approximate and is used only as a first estimate. A more accurate method of determining b is presented later.

Table 3-1

MATERIAL PROPERTIES AND TEST CONDITIONS FOR CNS DIRECT SHEAR TESTS[1]

Test	Uniaxial Compressive Strength, q_u (kN/m^2)	Normal Stiffness k_n ($kN/m^2/mm$)	Initial Normal Stress, σ_o (kN/m^2)	Base Friction Angle, ϕ_b (Degrees)	Initial Friction Angle, i_o (Degrees)	Asperity Height, h_m (mm)	Asperity Half Wave Length, λ (mm)
SM2	900	67.9	30	26	17.5	6.43	20.4
SM3	760	144.2	10	26	15.0	10.83	40.4
SM4	800	36.2	15	26	15.0	10.61	39.6
SM5	820	362.8	10	26	13.0	6.87	29.8
SM6	620	1374.0	10	26	14.0	5.48	22.0
SM7	750	222.5	20	26	18.5	6.26	18.7
SM8	750	222.8	10	26	15.5	6.33	22.8

[1]Data from Dight and Chiu (1)

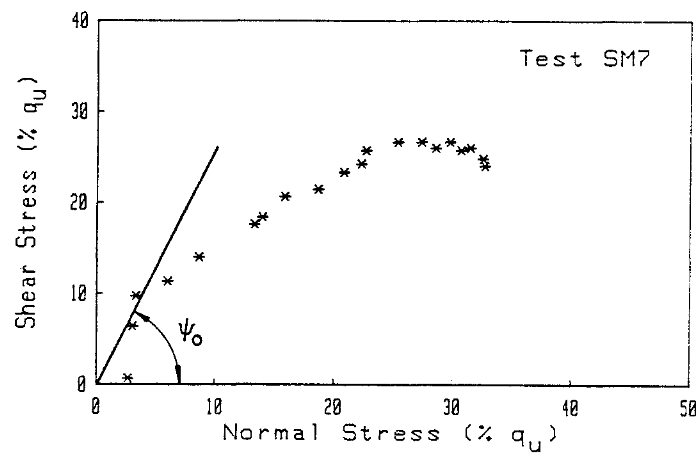

Figure 3-1. Stress Path for CNS Direct Shear Test SM7

After b has been estimated, the shear stress and normal stress data can be substituted into Equation 2-12 to calculate a_r. Note that as σ_n approaches 0, τ also approaches 0. Therefore a 0/0 condition is produced, and a small error in either σ_n or τ in this range of values can produce an unrealistic value of a_r. For this reason, the first one to three data points were excluded from the calculations.

Plotting ln a_r vs. displacement allows k_1 to be evaluated and the original calcu-

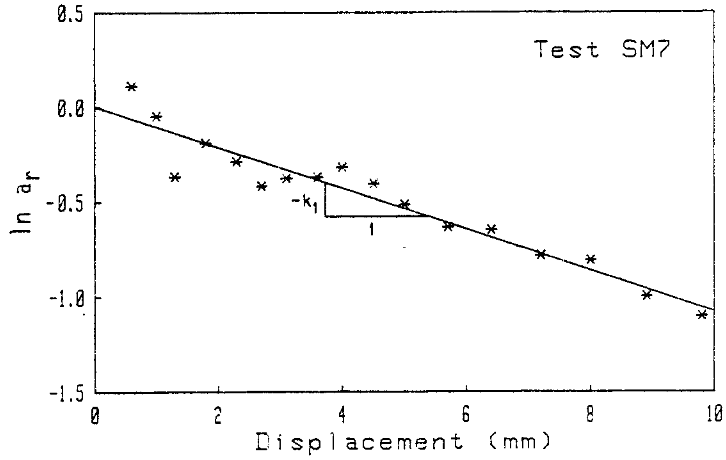

Figure 3-2. Determination of k_1

lation of b to be checked. The line through the data shown in Figure 3-2 was calculated from a least squares analysis. The value of the correlation coefficient, r, which was calculated from a regression analysis of displacement vs. ln a_r, shows that a linear relationship closely approximates the data of ln a_r vs. displacement. The constant k_1 is the negative slope of the line.

A more accurate method of determining b is based on the ln a_r intercept of the line shown in Figure 3-2. If the constant b is correct, the line should pass through ln $a_r = 0$ at zero displacement, indicating the interface is 100% intact before shearing commences. An intercept other than ln $a_r = 0$ indicates that the original determination of b was incorrect.

Changing the value of b and recalculating a_r has the effect of displacing the data vertically and altering the ln a_r intercept of the line while the slope remains constant. The constant b is determined by an iterative process of assuming a value, calculating a_r for all data points and finding the ln a_r intercept. Therefore, Figure 3-2 can be used to calculate k_1 and determine b indirectly.

Summary of Results

The calculated values for the constants k_1 and b, and the correlation coefficients for all seven tests, are summarized in Table 3-2. The values of k_1 are all within 12% of the mean value of 0.114. There are no apparent trends relating the variation of k_1 to material properties or test conditions, and the variation is attributed to experimental randomness. In a similar manner, the value of b varies by 17%

Table 3-2

SUMMARY OF RESULTS FOR CNS DIRECT SHEAR TESTS

Test	Empirical Coefficient b	Initial Rate of Shear Stress Increase, ψ_o (Degrees)	Rock Strength Component ϕ_r (Degrees)	Empirical Coefficient k_1 (1/mm)	Correlation Coefficient r
SM2	4.54	61.5	18.0	0.127	0.998
SM3	3.31	56.7	15.7	0.104	0.989
SM4	4.61	62.6	21.6	0.127	0.970
SM5	3.42	57.3	18.3	0.101	0.981
SM6	4.54	62.3	22.3	0.112	0.982
SM7	4.59	62.5	18.0	0.108	0.958
SM8	3.41	57.2	15.7	0.117	0.965
Mean	4.06		Mean	0.114	

from the mean value of 4.1. The magnitude of b should change from one test to the next because it is a function of the initial dilation angle, base friction angle, and strength of the teeth, all which vary from one test to the next. However, for these tests, ϕ_b was assumed to be constant, and the value of i_0 varied by only 5°. Therefore b is relatively constant in this case although, in general, it is expected to vary more widely.

As a check on the ability of the equations to model the progressive failure of joints, the constants summarized in Table 3-2 were used as input parameters for Equation 2-5 to generate the shear stress-displacement curve shown in Figure 3-3. Since k_1 was presented as a constant, the mean value of 0.114 was used. The value of b, on the other hand, should vary from test to test and the value presented in Table 3-2 was used. The dilations and normal stresses for these tests were modeled accurately by Dight and Chiu using Equation 2-16 with k_2 = 3.0, and their approach has been used in this analysis.

Since some of the constants used to generate the curve in Figure 3-3 were obtained from back-calculations of the data, the curve is not a prediction, but is a line of best fit based on Equation 2-5. The curve accurately models the data and can be extrapolated to predict behavior beyond the range of the data.

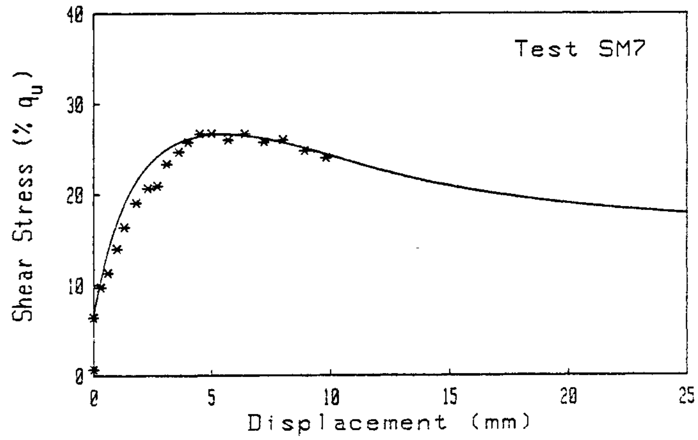

Figure 3-3. Shear Stress-Displacement Curve of Best Fit

SOCKET LOAD TEST ANALYSIS

In making the transition from modeling joints to socket wall interfaces, there are several important differences. First, the normal stiffness of rock sockets can only be estimated at this time. Second, the dilations and normal stresses can not be measured accurately to enable good relationships to be established. And third, the influence of certain field conditions, such as stress distribution and displacement with depth and material variability are difficult to quantify. Of these three differences, the most difficult to overcome is the second.

Williams (2) attempted to measure the interface dilation of rock sockets. However, only 5 out of a total of 21 tests gave consistent readings, and the interpretation of those values is questionable after the grout-rock interface displaces. Also, by multiplying the dilations reported by Williams by the normal stiffness of the socket, the resulting normal stress is unrealistically high. For these reasons, the dilations reported by Williams have not been used.

When the dilations and normal stresses are not known, the constants k_1, k_2, and b can not all be obtained from back-calculations of the data. However, if either the dilations or b and k_1 are known, the other quantities can be calculated.

To investigate the ability of the equations presented in Section 2 to model socket behavior, a series of 9 socket load tests conducted by Williams were analyzed. Table 3-3 summarizes the geometry and material properties for these tests as reported by Chiu and Dight (3).

Table 3-3

SUMMARY OF MATERIAL PROPERTIES FOR SOCKET LOAD TESTS[1]

Socket Test	Young's Modulus for Rock Material E_r (MN/m^2)	Normal Stiffness[2] k_n ($kN/m^2/mm$)	Poisson's Ratio for Rock Material ν_r	Uniaxial Compressive Strength q_u (kN/m^2)	Socket Length L (m)	Socket Diameter D (m)	Base Friction Angle ϕ_b (Degrees)	Initial Dilation Angle i_o (Degrees)	Asperity Height h_m (mm)	Asperity Half Wave Length λ (mm)
S3	420	670	0.26	780	2.51	1.17	26	18.5	26.6	79.5
S5	410	680	0.26	830	2.59	1.12	26	16.7	16.5	55.0
S15[3]	75	355	0.26	820	0.87	0.40	26	12.0	10.0	50.0
M1[4]	275	495	0.19	1750	2.0	1.22	26	18.1	12.6	37.4
M2	190	300	0.20	1550	2.0	1.30	26	31.1	40.1	66.5
M3	650	1070	0.20	1550	2.0	1.23	26	15.6	20.2	75.5
F1	840	1670	0.18	2400	1.0	1.21	26	14.4	12.0	44.1
F2	370	665	0.20	2250	1.0	1.21	26	10.2	8.2	45.6
WG	980	1310	0.17	2800	2.0	1.58	26	25.8	41.4	85.7

[1]Data from Chiu and Dight, (3) [3]Interface shaped to a regular triangular profile
[2]From finite element analysis by Chiu and Dight, (3) [4]Cast under bentonite

The sockets were installed in Melbourne mudstone, which is the same rock material as the CNS direct shear tests analyzed in the previous section. Because the rock material is the same, the empirical constants evaluated from the direct shear tests should also be the same.

If the constants from the CNS direct shear tests summarized in Table 3-2 are used as input parameters for Equation 2-5 to predict the force-displacement behavior, a rather poor result is obtained. A typical prediction is illustrated in Figure 3-4 from test M3. The predicted curve has two problems: (1) the peak occurs at a small displacement, and (2) the strength is significantly underpredicted, indicating either that the values of some of the constants are in error, or the equations do not model the behavior.

By changing the value of ψ_0, from which b is calculated, the initial slope is altered, but the prediction of strength is unchanged. For this reason, it is unlikely that an incorrect value of b is responsible for the deficiencies outlined above.

By assuming k_1 = 0 and recalculating the stress-displacement curve, a better fit is obtained. However, k_1 = 0 implies that the interface does not degrade and become smoother with displacement. This is unlikely unless the normal stress is at the

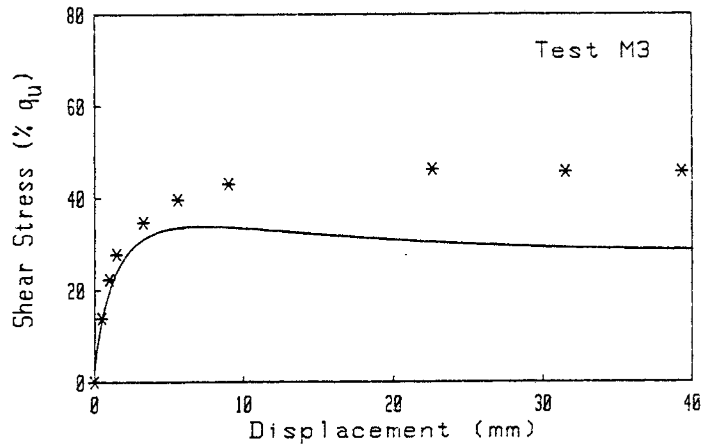

Figure 3-4. Prediction of Socket Behavior Using Initial Assumptions

transition stress and new fractures are being generated in preference to sliding along pre-existing breaks.

Although the magnitude of the dilations measured by Williams is probably in error, the data give insight into the trends to expect. By comparing the measured dilations with the predictions, it is observed that the measured values tend to increase more slowly and peak with greater displacement. The predictions peak too fast in comparison, and fall short of the measured values. These are the same trends noted by comparing the predicted shear stresses with the measured values, from which it is concluded that the dilation and normal stress predictions are in error. Note that the dilations and normal stresses differ only by the normal stiffness of the socket wall.

To obtain more realistic values for the dilations and normal stresses, σ_n was back-calculated from Equation 2-5 using the shear stress vs. displacement data. Since σ_n appears in Equation 2-5 both as an exponent and a coefficient, there is no explicit solution, and an iterative approach has been adopted. The value of k_1 was assumed constant at 0.114 and b was calculated from Equation 2-10 assuming ϕ_r = 15°, ϕ_b = 26°, and i_o from Table 3-3.

Figure 3-5 compares the back-calculated dilations for socket M3 with the predicted dilations. The poor result is typical for the entire set of nine socket tests. An attempt was made to model the data by changing the value of k_2 in Equation 2-16; however, this changed only the magnitude of the dilations and had little effect on the shape of the curve. The data are modeled more accurately by changing the form

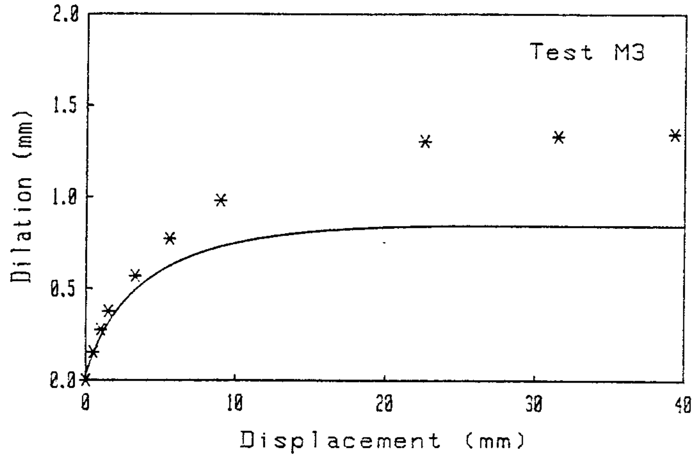

Figure 3-5. Comparison of Back-Calculated Dilations with Predictions Based on Equation 2-16

of the rate of dilation equation from a power function to an exponential function given by:

$$\dot{u} = \tan i_o \exp \left(-k_5 \frac{\sigma_n}{\eta\, q_u}\right) \tag{3-1}$$

in which k_5 = empirical constant.

This function has been normalized against q_u, similar to Equation 2-16, and starts at $\dot{u} = \tan i_o$ for $\sigma_n = 0$ and degrades to 0 at displacement = λ. The advantage of Equation 3-1 is that the dilations increase more slowly and peak later, ultimately achieving a higher maximum and thereby modeling the data more accurately.

There is difficulty in performing a least squares fit of dilations from Equation 3-1 to the back-calculated dilations because Equation 3-1 is a differential equation which has not been solved explicitly. Therefore, the fit is a trial and error process of assuming a value for k_5, graphing the curve, and observing the agreement with the data. A summary of k_5 determined from this procedure is presented in Table 3-4.

Figure 3-6 shows the results for Test M3, with the dilation vs. displacement curve from Equation 3-1 superimposed on the back-calculated dilations. The plots of the

Table 3-4

SUMMARY OF RESULTS FOR SOCKET LOAD TESTS

Socket Test	Empirical Coefficient b	Initial Rate of Shear Stress Increase ψ_o (Degrees)	Empirical Coefficient k_1 (1/mm)	Empirical Coefficient k_5
S3	3.87	59.5	0.114	1.5
S5	3.50	57.7	0.114	2.0
S15[1]	2.69	53.0	0.114	1.5
M1[2]	3.79	59.1	0.114	2.3
M2	8.35	72.1	0.114	2.3
M3	3.29	56.6	0.114	2.6
F1	3.08	55.4	0.114	2.0
F2	2.28	51.2	0.114	--
WG	5.91	66.8	0.114	6.0

[1]Interface shaped to a regular triangular profile
[2]Cast under bentonite

remaining eight tests are presented in Appendix B and, in general, show good agreement with the data, except for Test F2.

For Test F2, the dilation, or in this case apparent dilation, rises very rapidly with very little displacement. Since the dilations were back-calculated from the shear stress data, they reflect inconsistencies in the data. The rapid rise in the dilation is attributed to an initial bond at the interface which caused the shear stress to increase rapidly with very small displacements. Because of the inconsistencies in the data for Test F2, a value of k_5 has not been reported.

To check on the ability of Equations 2-5 and 3-1 to model socket behavior accurately, a curve of best fit was calculated and compared to the data. Figure 3-7 presents this curve for Test M3, while the comparisons for the remaining eight tests are given in Appendix B. The correspondence between the measured data and the model curve is good, with the trends of the data and strength modeled well.

PREDICTION OF BEHAVIOR

The previous sub-sections have demonstrated that socket wall interfaces can be

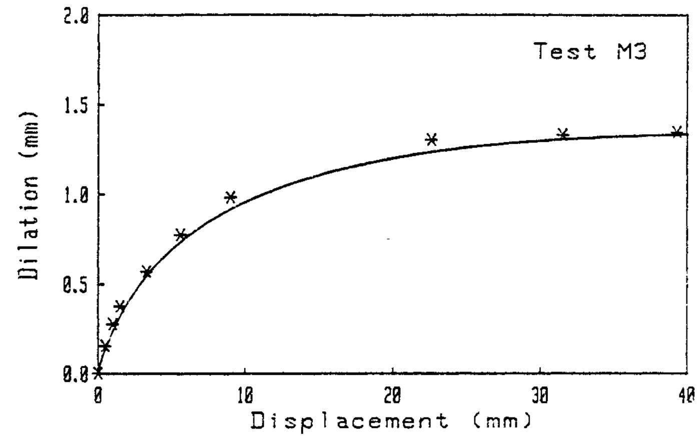

Figure 3-6. Modeling Dilations for Shear Socket M3 Using Equation 3-1

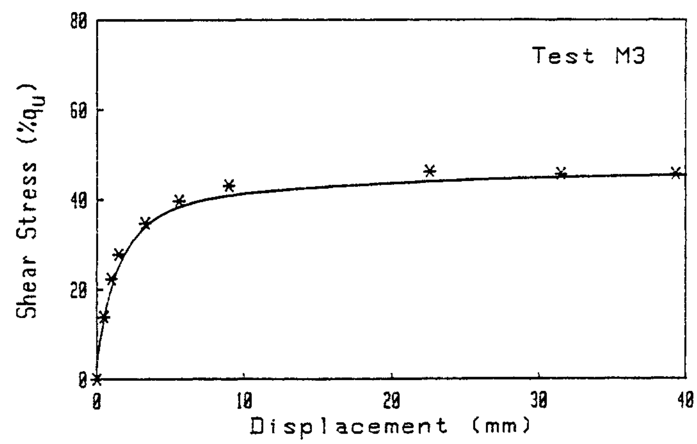

Figure 3-7. Shear Stress-Displacement Curve of Best Fit for Shear Socket M3

modeled as dilatant rock joints with the equations presented in Section 2 with the modification of using Equation 3-1 to model dilations. The data base established in these sections now can be applied to other systems to predict socket behavior. However, it should be noted that the data base is very limited and represents a narrow range of conditions.

As an example of the application of these methods, a set of three socket pullout tests reported by Webb and Davies (4) has been examined. All three sockets were augered with the same techniques at the same site, so the interfaces are expected to have similar characteristics. The shear stress-displacement data for all three

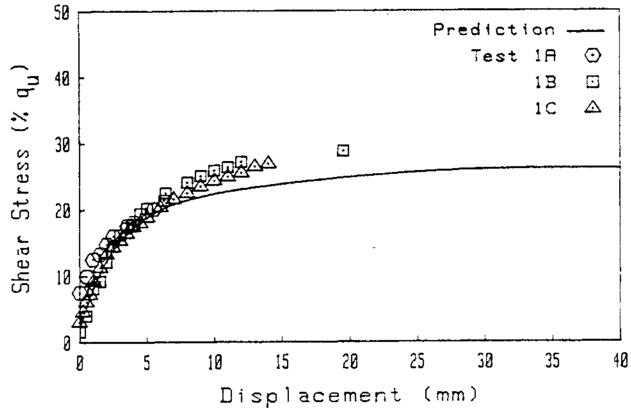

Figure 3-8. Prediction of Socket Behavior and Capacity for Tests by Webb and Davies (4)

tests is presented in Figure 3-8 and show nearly identical behavior.

The sockets were installed in laminated fine to medium-grained sandstone beneath 8 m of clay. The upper 8 m of the holes were overcored and cased to prevent the transfer of shear stress. Table 3-5 summarizes the socket geometry and material properties.

Table 3-5

SOCKET GEOMETRY AND MATERIAL PROPERTIES FOR SOCKET LOAD TESTS[1]

Socket Test	Length L (m)	Diameter D (m)	Uniaxial Compressive Strength q_u (kN/m²)	Young's Modulus for Material E_r (MN/m²)	Young's Modulus for Rock Mass[2] E_m (MN/m²)	Normal Stiffness k_n (kN/m²/mm)
1A	1.08	0.471	2500	100	80	295
1B	1.75	0.450	2500	100	80	309
1C	2.77	0.450	2500	100	80	309

[1]Data from Webb and Davies (4)
[2]Estimated from E_r
[3]From Equation 2-14 assuming $\nu_m = 0.15$

Table 3-6

VALUES OF COEFFICIENTS FOR SOCKET LOAD TESTS

Symbol	Parameter	Value	Method Used to Acquire Value
i_o	Initial dilation angle	20°	Estimate from Tables 3-1 and 3-3
ϕ_b	Base friction angle	26°	Estimate from Table 3-1
ϕ_r	Initial rock strength component	15°	Estimate from Table 3-2
ψ_o	Initial rate of shear stress increase	61°	Summation of i_o, ϕ_b, and ϕ_r
b	Coefficient for Equation 2-5	4.2	Calculated from ψ_o
λ	Asperity half wave length	50 mm	Estimate from Tables 3-1 and 3-3
k_1	Empirical coefficient, Equation 2-6	0.114/mm	Average of values in Table 3-2
k_5	Empirical coefficient, Equation 3-1	2.0	Estimate from Table 3-4

The rock mass elastic modulus, E_m, of 80 MN/m^2 listed in Table 3-5 represents a 20% reduction from the Young's modulus for the rock material. This reduction factor is an estimate based on the fact that the formation is a laminated sandstone, and that there was a 100% core recovery from test borings at the site.

The values of the key terms necessary to model the sockets are presented in Table 3-6 and were obtained from summaries of those terms in Tables 3-1 to 3-4. Figure 3-8 presents the prediction of behavior using the estimated values for these terms, and compares the prediction with the load test data. From this figure it is seen that both the strength of the socket and its behavior are predicted well. The good agreement illustrates the ability of the equations to model the rock socket behavior.

SENSITIVITY STUDY

The input parameters for the predictions are characterized by ranges in values, as opposed to precise numbers. When predictions are made, the effects of variations in these parameters should be evaluated. The following uses the expected ranges for each of the six input parameters to calculate changes in the predictions. Each of the six parameters was assumed to vary independently while the other five were kept constant. The results of this study are presented in Figures 3-9 to 3-14.

The greatest changes in the predicted capacity come from altering the values of k_n and i_o; there is a one to one correspondence between changes in the value of these parameters and the predicted capacity. Doubling the value of either parameter

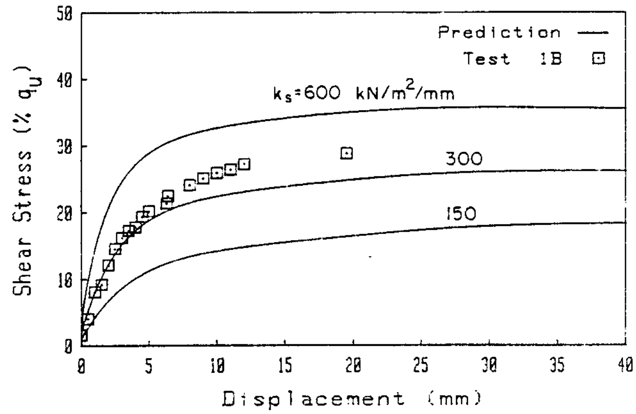

Figure 3-9. Sensitivity of Prediction to Changes in Normal Stiffness, k_n

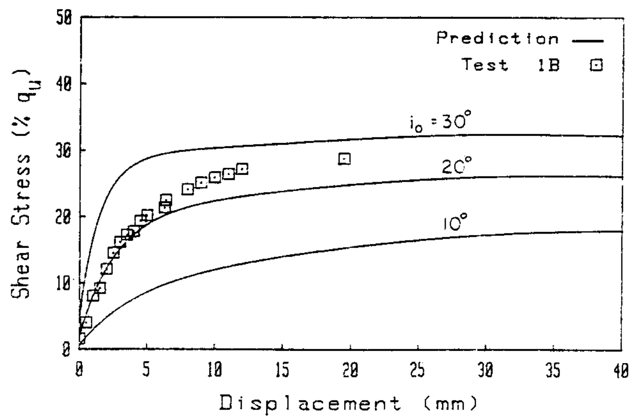

Figure 3-10. Sensitivity of Prediction to Changes in Initial Dilation Angle, i_o

approximately doubles the capacity, and halving the value decreases the capacity by about 50%. The shapes of the curves remain basically unchanged. It is understandable that changes in k_n or i_o alter the capacity drastically because both are used directly to calculate the normal stress, which controls the capacity.

Examination of the curves for variations in k_5 and λ shows similar changes in capacity and behavior. A 50% change in either parameter corresponds to about a 25% change in capacity. Changes in λ have little effect on the initial steep portion of the curve, but the deviation becomes more noticeable with increasing displacement. The parallel trend observed from altering the value of these parameters can

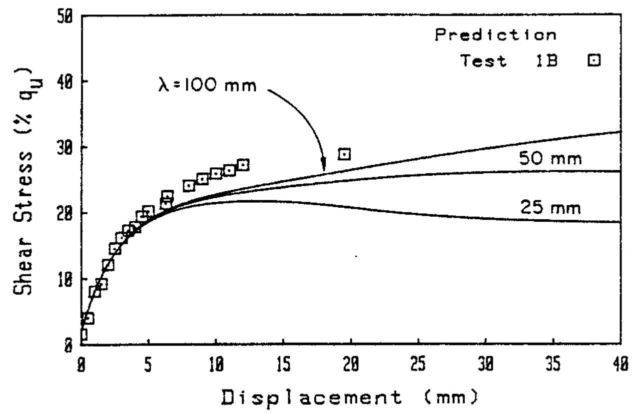

Figure 3-11. Sensitivity of Prediction to Changes in Asperity Half Wave Length, λ

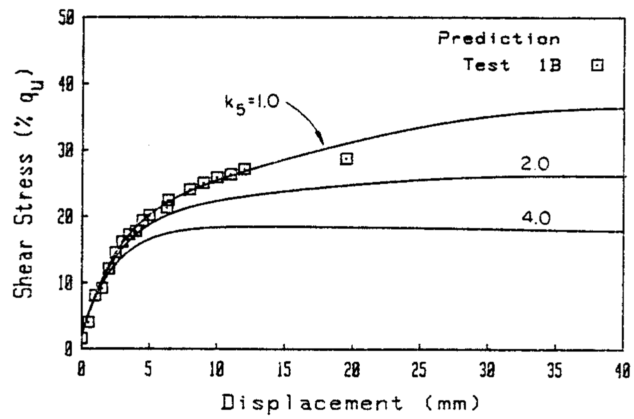

Figure 3-12. Sensitivity of Prediction to Changes in Empirical Coefficient, k_5

be seen by looking at the rate of dilation equation:

$$\dot{u} = \tan i_o \exp\left(-k_5 \frac{\sigma_n}{(1 - \Delta y/\lambda)\ q_u}\right) \tag{3-2}$$

from which it is seen that increasing λ has a similar effect to decreasing k_5, and vice versa.

The final two parameters of interest are ϕ_b and k_1. Altering either of these parameters has relatively little effect on the capacity. This is reasonable because capacity, as described herein, is primarily a function of normal stress, and

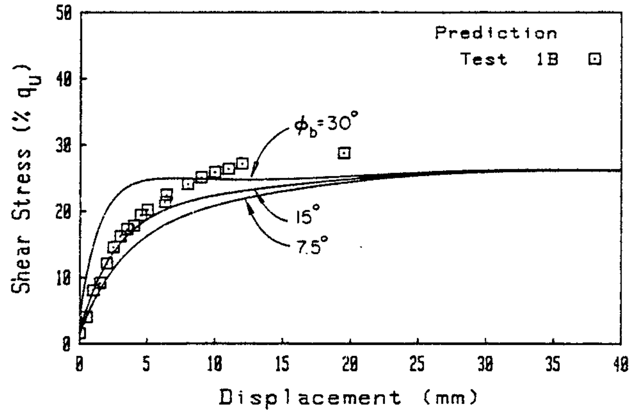

Figure 3-13. Sensitivity of Prediction to Changes in Rock Strength Component, ϕ_b

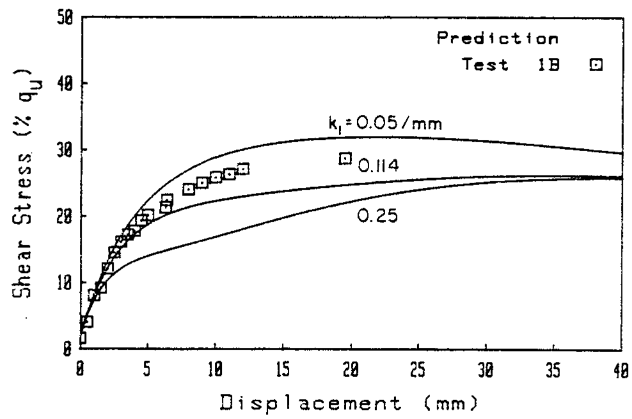

Figure 3-14. Sensitivity of Prediction to Changes in Empirical Coefficient, k_1

neither parameter is included in the calculation of the normal stress.

Although variations in either k_1 or ϕ_b have little effect on ultimate capacity, they do change the behavior at smaller loads and displacements. For displacements of 3 mm to 20 mm, the prediction of shear stress changes by about 30% when the values of k_1 or ϕ_b are doubled or halved.

SUMMARY

In Section 2, equations were developed which described the grout-rock interface behavior of rock anchors and sockets. In this section, these equations were applied to three sets of test data which included a set of constant normal stiffness direct shear tests and two sets of socket load tests from different locations. The analysis of the direct shear tests showed that the equations model grout-rock interfaces well under laboratory conditions. A data base of empirical constants also was developed from back-calculations of these data.

The equations presented in Section 2, along with the data base of empirical constants, were used to model the grout-rock interfaces of sockets with poor results. However, by changing the form of the rate of dilation equation from a power function (Equation 2-16) to an exponential function (Equation 3-1), good agreement was observed between the curve of best fit and the actual data.

The socket load test data also were used as a basis for evaluating the sensitivity of the predictions to variations in the input parameters. The results showed a one to one correspondence between variations of some parameters and socket capacity, and little correspondence with variations of other parameters.

REFERENCES

1. Dight, P. M. and Chiu, H. K., "Prediction of Shear Behavior of Joints Using Profiles," International Journal of Rock Mechanics and Mining Sciences, Vol. 18, No. 5, Oct. 1981, pp. 369-386.

2. Williams, A. F., "The Design and Performance of Piles Socketed into Weak Rock," Ph.D. Thesis, Monash University, Australia, 1980, (as referenced by Chiu and Dight, 3).

3. Chiu, H. K. and Dight, P. M., "Prediction of the Performance of Rock-Socketed Side-Resistance-Only Piles Using Profiles," International Journal of Rock Mechanics and Mining Sciences, Vol. 20, No. 1, Feb. 1983, pp. 21-32.

4. Webb, D. L. and Davies, P., "Ultimate Tensile Loads of Bored Piles Socketed into Sandstone Rock," Proceedings, International Conference on Structural Foundations on Rock, Vol. 1, Sydney, 1980, pp. 265-270.

Section 4

ANALYSIS OF ROCK MASS UPLIFT FAILURE

Sections 2 and 3 focused on the behavior of sockets and anchors failing by grout-rock interface slip. This section examines the second, and less common, failure mode associated with geotechnical engineering, that of rock mass uplift. To investigate the rock mass uplift failure mode, a series of nine anchor pullout tests conducted by Bruce (1) have been examined. Of these nine tests, seven failed by rock mass uplift and two failed by grout-rock interface slip. The material properties for the anchors failing by rock mass uplift or grout-rock interface slip are summarized in Table 4-1. Table 4-2 gives the geometry, capacity, and failure modes.

ELASTIC BEHAVIOR

As an illustration of the use of the elastic solutions presented in Section 2, the computed axial stress distributions have been compared with those measured by Bruce (1). In the elastic range, the anchor properties having the greatest influence on behavior are the relative stiffnesses of the grout and rock mass, and the length to diameter ratio. For these tests, the stiffness ratio, $K_E = E_g/E_m$, is about 3 which places the stress distributions in the middle of those presented in Figure 2-4. The length to diameter ratios are about 13 and 20 for anchors 6 and 53, respectively. These ratios are significantly higher than those analyzed and presented in Figure 2-4, which means that a direct comparison can not be made; however, the trends are similar.

Figures 4-1 and 4-2 present the axial stress distributions at low loads for anchors 6 and 53, respectively. Both show a rapid decrease in axial stress within the first 0.25 m of the surface. This is followed by a slower rate of axial stress decrease to a depth of 0.75 m to 1 m. Below this depth the remaining axial stress is dissipated more rapidly and approaches zero at the tip.

By comparing the measured stress distributions in Figures 4-1 and 4-2 with those calculated from elastic methods, presented in Figure 2-4, two observations can be made. First, the elastic solutions show a rapid decrease of axial stress near the

Table 4-1

MATERIAL PROPERTIES FOR ANCHOR PULLOUT TESTS[1]

a. Rock Mass	
Material	Thinly bedded shaley sandstone
Elastic modulus[2]	10 GN/m^2
RQD	75%
Fractures/meter	8

b. Rock Material	
Point load strength	2.5 MN/m^2
Uniaxial strength[3]	60.0 MN/m^2
Young's modulus	25 GN/m^2
Poisson's ratio	0.2

c. Grout	
Material	Ferrocrete
Water/cement ratio	0.45
Cube strength	50 MN/m^2
Uniaxial strength[4]	45 MN/m^2
Young's modulus[5]	32 GN/m^2

[1]Data summarized from Bruce, (1)
[2]From Goodman jack
[3]Estimate from point load strength
[4]Estimate from cube strength
[5]Estimate from uniaxial strength

surface similar to the measured data. Second, the shape of the theoretical axial stress distribution curve is smooth and concave to the right in comparison to the convex bulge seen in the measured curve. This bulge indicates that more stress is being transferred to the 1 m depth than the elastic solutions predict.

The high axial stress at a depth of 1 m can be explained by either malfunctioning strain gages, cracking of the grout, partial pullout of the tendons from the grout, or by the influence of hard or soft zones within the rock mass. The first three explanations must be investigated at the test site and therefore can not be considered here. Attributing the unexplained behavior to changes within the rock mass assumes that the axial stress distributions are dependent upon the relative stiffnesses of the grout and rock mass, and variations in the stiffness would cause changes in the stress distribution.

Table 4-2

GEOMETRY AND FAILURE MODES FOR ANCHOR PULLOUT TESTS[1]

Anchor	Length (m)	Diameter (m)	Failure Mode	Capacity (kN)
1	0.75	0.114	Rock mass uplift	440
2	0.75	0.114	Rock mass uplift	500
3	0.75	0.114	Rock mass uplift	450
4	1.50	0.114	Rock mass uplift	1495
6	1.50	0.114	Rock mass uplift	1206
23[2]	1.50	0.114	Rock mass uplift	1834
24[2]	1.50	0.114	Rock mass uplift	1594
52	2.25	0.114	Interface slip	1978
53	2.25	0.114	Interface slip	1891

[1]Data summarized from Bruce (1)
[2]Underreamed

Data presented by Bruce (1) show that a soft mudstone bed intersects the anchor at a depth of about 1 m. Although detailed information on the thickness and stiffness of the bed, and changes in the sandstone above and below the bed are unavailable, the presence of the bed itself indicates that the sandstone formation is not homogeneous and differences are likely.

The preceding illustrates the need to apply engineering judgment when using elastic solutions and finite element models. These models are based on the assumption of a linear elastic material and a homogeneous medium. Actual foundations rarely fulfill these assumptions, so the theoretical solutions are useful, but only approximate.

INELASTIC BEHAVIOR

In the analysis of the grout-rock interface slip failure mode, the rock mass was

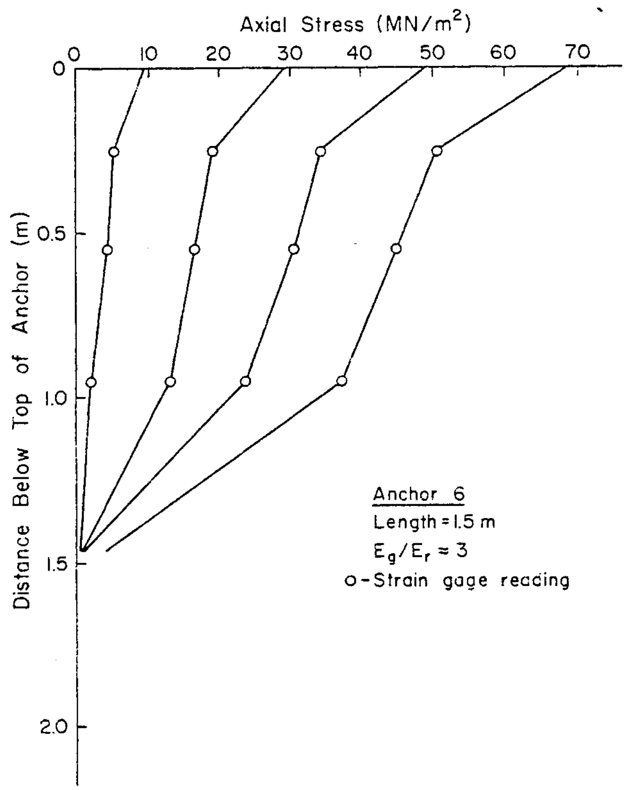

Figure 4-1. Axial Stress Distribution Along Anchor 6

Source: Reference (1), p. 294.

assumed to be intact and elastic. Inelastic displacements occurred only by slip along the grout-rock interface. In contrast to these systems, the behavior of systems failing by rock mass uplift is characterized by inelastic deformations in the rock mass while the grout rock interface remains intact.

The behavior of the rock mass during uplift failure can be evaluated by examining a vertical cross-section of an anchor and adjacent rock mass after failure, as shown in Figure 4-3 for anchor 3. Permanent voids opened near the rock surface, close to the anchor, which created a zone of loosened rock surrounding the anchor. The degree of loosening is maximum near the anchor butt and decreases both radially and with depth.

Design for rock mass uplift often assumes that a failure surface in the shape of an inverted cone develops around the anchor. The cone is assumed to be intact and its

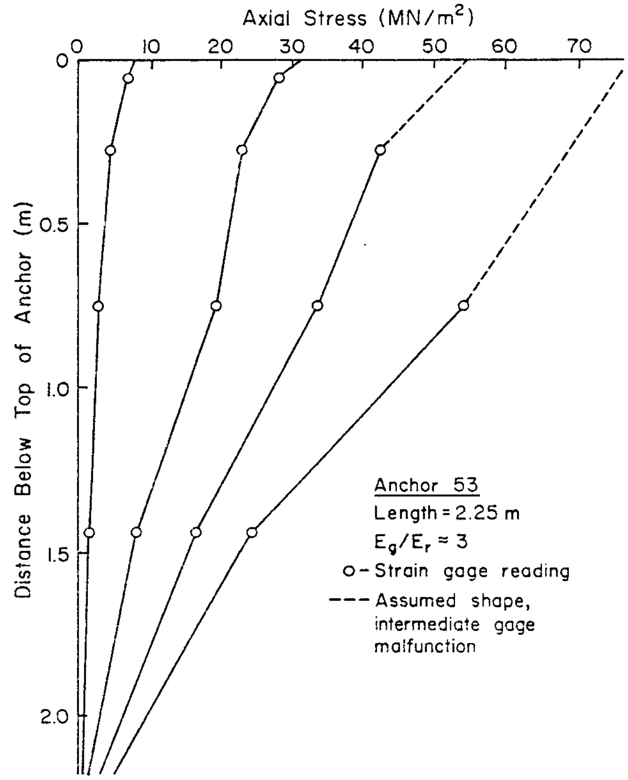

Figure 4-2. Axial Stress Distribution Along Anchor 53

Source: Reference (1), p. 315.

weight is taken as the anchor capacity. Observations from Figure 4-3 that the rock mass is extensively cracked, and that the degree of cracking changes with location, indicate that the assumption of an intact cone lifting out is only a rough approximation. Although the zone of loosened rock is approximately conical, it is not intact, and it does not lift up as an intact mass. The true failure mechanism is a complicated combination of shear along joint planes, movement of discrete blocks, and tensile failure of the rock material. Until better information is available, a more detailed analysis is not possible.

The different degrees of loosening shown in the vertical cross-section are also seen in the plan view of the crack pattern. Figure 4-4 shows the progression of surface cracking with increasing loads for anchor 6. For loads less than 400 kN, the system is in the elastic stage and there is no surface cracking. Above 400 kN, cracks develop near the anchor and begin to radiate outward from the anchor, gen-

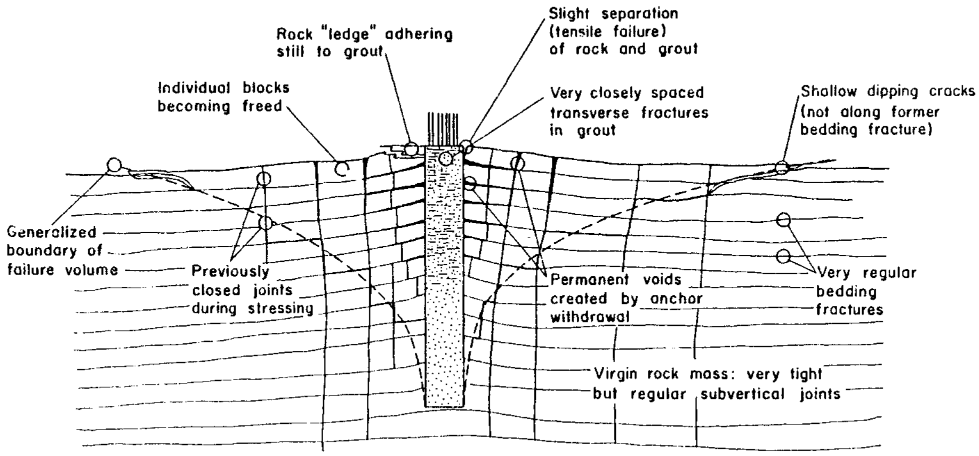

Figure 4-3. Vertical Cross-Section of Failed Anchor 3

Source: Reference (1), p. 276.

erally following the two sets of natural discontinuities. The loads are shown in Figure 4-4 by the small index numbers near the cracks, indicating the load at which the crack formed.

With increasing loads, the fractures continued to radiate outward. The fact that cracks grew with increasing loads also tends to discount the intact cone failure mechanism. The dotted line enclosing the anchor and cracks represents a circumferential fracture set which developed at failure, after the radial cracks progressed outward to that point.

The footings which support the loading frame impose a concentrated surcharge at the locations indicated in Figure 4-4. The increased surcharge effectively overcomes the applied tensile stresses and prevents the development of cracks near that region. This influence is seen by the elongated shape of the surface crack pattern.

In comparison with anchor 6 which failed by rock mass uplift, Figure 4-5 presents the surface crack pattern for anchor 53 which failed by grout-rock interface slip. The same basic trends are noted for these two anchors at loads less than the failure load. For anchor 53, no cracks developed in the elastic range with loads under 900 kN. Increasing loads correspond to radial crack growth, especially parallel to the natural discontinuities. The primary difference between anchors 6 and 53 is that a circumferential crack set developed around anchor 6 but not around anchor 53. The explanation for this behavior is that the grout-rock interface slipped

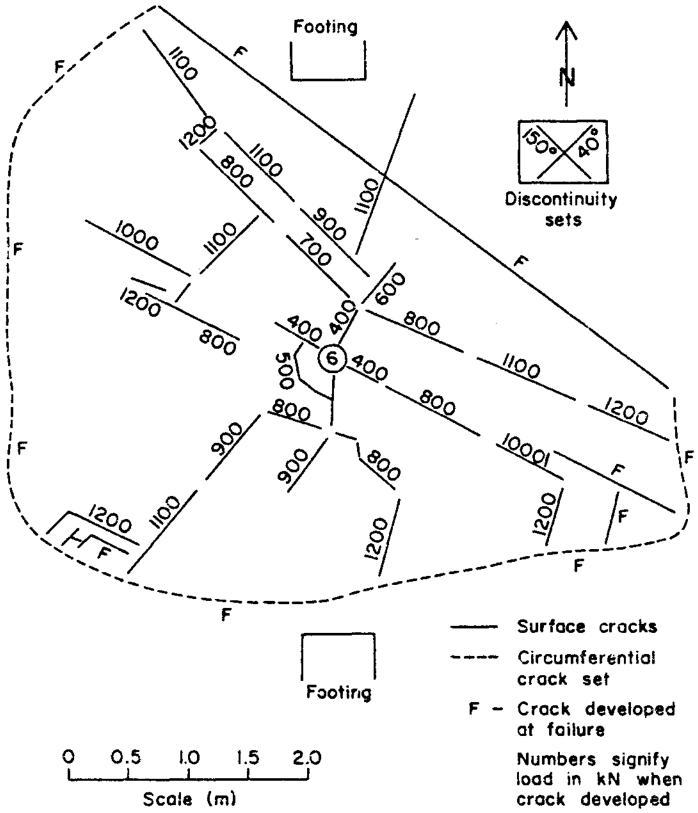

Figure 4-4. Rock Surface Fracture Pattern for Anchor 6

Source: Reference (1), p. 273.

before rock mass uplift could occur.

The fact that the pre-failure crack patterns for the two anchors are similar indicates that similar mechanisms are at work. For this reason, the two failure modes can not be considered to be completely independent at shallow depths. In both cases, cracking and loosening of the rock mass at least contributed to failure and may have been the primary failure mechanism.

DESIGN CRITERIA

The design for rock mass uplift commonly is based on the weight of a conical section of rock uplifting with the anchor. In sound homogeneous rock, the cone is assumed to have a vertex at the anchor tip and enclose an angle of 90°. For weathered, weak, or highly jointed rock masses, a cone with its vertex at one half the total anchor depth and enclosing an angle of 60° is more common. Although the

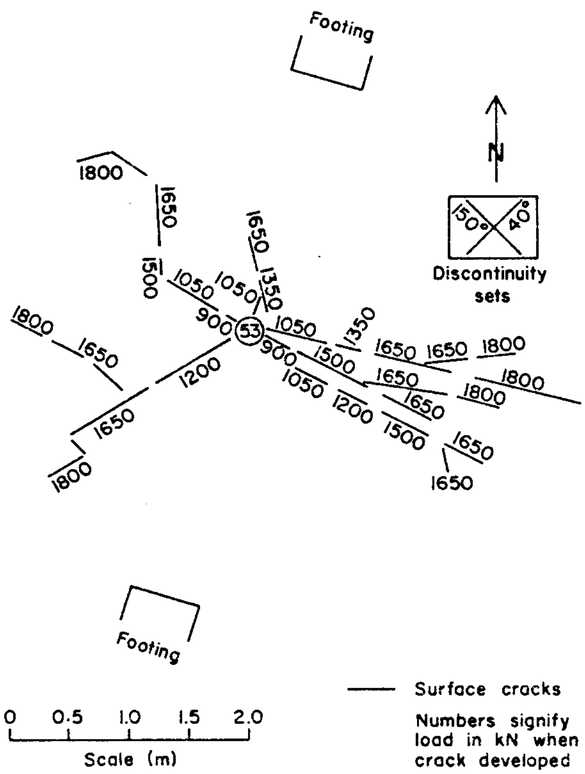

Figure 4-5. Rock Surface Fracture Pattern for Anchor 53

Source: Reference (1), p. 302.

total anchor depth and enclosing an angle of 60° is more common. Although the failure mechanism assumed by this method is not correct, the method gives an estimate of capacity for design with shallow anchors. This method is conservative, but the conservatism is necessary to account for uncertainties.

A second method of evaluating the uplift capacity of anchors is with empirical equations. Researchers have presented several different forms of these equations, and all are functions of depth of embedment. Bruce (1) found that a parabolic equation fit his data well. Bruce's equation is:

$$P = 6\ D^2 \tag{4-1}$$

in which P = capacity in kN and D = depth of embedment in meters.

With increasing depth, failure by rock mass uplift grades into interface slip and is no longer the controlling failure mode. Therefore, the two methods of evaluating anchor capacity for uplift failure are limited to shallow cases. For the tests by Bruce, the transition from uplift failure to interface slip occurred at a depth of about 2 meters.

SUMMARY

The uplift failure of anchors occurs only in the case of shallow anchors installed in highly fractured rock masses. For the tests by Bruce, the uplift failure mode occurred only in those anchors 2 m deep or less. The failure mechanism appears to be associated with progressive loosening of the rock mass around the anchor, with ultimate failure occurring only after the rock mass is extensively cracked and loosened.

Similar mechanisms of cracking and loosening of the rock mass control the behavior of shallow anchors failing by grout-rock interface slip. At shallow depths, there is a progression from rock mass uplift failure to interface slip. The initial behavior of these systems is the same, and only the final failure mechanism changes.

REFERENCE

1. Bruce, D. A., "The Design and Performance of Pre-stressed Rock Anchors with Particular Reference to Load Transfer Mechanisms," Ph.D. Thesis, University of Aberdeen, Scotland, Oct. 1976, 670 p.

Section 5

SUMMARY AND CONCLUSIONS

SUMMARY

Rock anchors and sockets are multi-component foundation systems, which can fail in either of four modes: (1) structural failure of the anchor bar or tendon, (2) bond failure along the interface between the bar or tendon and the grout, (3) failure along the grout-rock interface, and (4) uplift failure of the rock mass. Modes 1 and 2 are structural problems which are addressed by appropriate steel and concrete design criteria. Modes 3 and 4 are geotechnical concerns. Mode 3 failure is the most dominant, while mode 4 failure occurs only for very specific geometric and rock conditions. Using available theoretical and experimental data in the literature, a general model has been developed for evaluating the geotechnical behavior of rock anchors and socket systems. Particular emphasis has been placed on the mode 3 mechanisms.

The general behavioral patterns were described in Section 1, as well as current design practices. Guidelines were also given for evaluating the mode 1 and 2 failure mechanisms.

In Section 2, the grout-rock interface was examined as a progression through three stages of behavior from elastic, to secondary, and finally to residual. For each stage, the equations governing the capacity and behavior were developed. The elastic stage was characterized as an intact system which can be analyzed using elastic solutions and finite element models. The secondary stage was characterized by a failure surface along the grout-rock interface. The capacity and behavior during the secondary stage were based on the magnitude of displacement along the slip surface and the character of the interface. The character of the interface was quantified in terms of triangular teeth with an effective size and dilation angle. It was noted that roughness is a variable with limits of smooth and interlocking. The third stage is the residual condition, characterized by total degradation of the slip surface. This condition is achieved only after the system has experienced large displacements.

Section 3 evaluated the methods and concepts developed in Section 2. First, a series of constant normal stiffness direct shear tests on concrete-mudstone interfaces were analyzed. Measurement of the dilation and normal stress allowed the values of the constants to be back-calculated. By applying the values of the parameters to socket load tests, the analysis procedure and equations were refined and a more extensive data base was developed. With the equations and constants already described, and estimates of the other parameters, the behavior of a series of three instrumented socket pullout tests was modeled with good results. The same set of data was used to investigate the sensitivity of the method to changes in the input parameters.

In Section 4, the limits of applicability and transition into the rock mass uplift failure mode were investigated by analyzing a series of anchor pullout tests. It was noted that rock mass uplift is associated with progressive cracking and loosening of the rock mass, and that there is a gradual transition from the rock mass uplift to interface slip failure mode with increasing depth. For these reasons, shallow sockets failing by interface slip are affected adversely by proximity to the surface.

CONCLUSIONS

The methods of analysis presented are based on both theoretical concepts and observations of actual socket behavior. Throughout the development process, examples of behavior were presented for clarity and to support the concepts. The practicality of the method was demonstrated by applying the concepts to field load tests. These applications also served to verify the ability of the method to model the behavior accurately.

The information necessary to evaluate socket performance includes the material properties, characteristics of the grout-rock interface, and values of several empirical constants. The material properties, such as rock strength and rock mass elasticity, can be obtained easily from field and lab testing. Quantification of the socket wall roughness in terms of the dilation angle and size of the asperities is achieved by direct measurement techniques in which the interface profile is digitized and analyzed, or from correlations with a standard set of joint roughness profiles.

In addition to the information which can be obtained directly by measurement or testing, several empirical constants must be evaluated. These include b, k_1, and k_5 which must be back-calculated from load test data, or estimated from sockets tested in similar conditions. Additional data will be necessary to generalize these constants for routine practice.

LIMITATIONS

Although the preceding presents a comprehensive description of rock socket behavior, there are additional factors which influence behavior. Following is a summary of factors which influence the behavior, either directly or indirectly:

1. The elastic modulus of the rock mass and normal stiffness of the socket both increase with depth. This occurs because the confining stress increases with depth and near-surface effects are minimized. The sensitivity study showed that changes in the normal stiffness directly influenced both the normal stress developed at the interface and the shear stress capacity. Because of these changes in normal stress and and shear stress with depth, a nonuniform stress distribution results.

2. The analysis assumed identical behavior for uplift and compression loading, except for near-surface uplift failure and loosening effects. It is expected that compression loading would result in a greater capacity because of Poisson's ratio effects and the closing of discontinuities, which would stiffen the system.

3. Repeated cycles of loading may soften the load-displacement response and reduce the capacity. This effect could be described as a degradation of the grout-rock interface, and can be accounted for by reducing the value of the area reduction ratio.

4. Because foundation elements are not rigid, the foundation butt experiences more deformation than the tip. In the secondary stage, deformations control the shear stress capacity of the interface, and it is expected that the larger deformations at the butt cause higher normal stresses to develop and the shear stress to increase. This effect would result in a nonuniform stress distribution with depth.

RECOMMENDATIONS FOR FURTHER RESEARCH

There are two aspects of rock socket and anchor behavior which are not well understood and could benefit from additional research. These are the failure mechanisms and capacity of anchors failing by rock mass uplift, and the dilations and normal stresses developed by displacement along the grout-rock interface. Research into the dilations and normal stress generated during shearing is necessary both in the areas of roughness characterization and of the actual dilations generated.

Quantification of the socket wall roughness is based on an idealized triangular profile obtained by direct measurement or empirical methods. This method works well for analysis purposes, but the procedures used to evaluate i_o and λ can be difficult to implement in practice. Measuring and analyzing the surface profiles is necessary for research, but a more practical method is needed for design purposes. Summaries of i_0 and λ referenced to rock type, rock strength, and drilling method could provide a useful correlation.

The field pullout tests by Williams showed that the actual dilations of socket walls are difficult to measure and interpretation of the results is subjective. It is unfortunate that good data on the magnitude of dilation generated during shearing are unavailable because capacity is related directly to the dilation and resulting normal stress. Methods of measuring the actual dilations and normal stresses need to be developed.

The available data on rock mass failure of anchors in uplift are useful but have a limited range of application. Bruce and others have addressed this aspect of socket and anchor behavior at specific sites and under specific test conditions. This information alone is not adequate to develop a good understanding of the uplift failure mode, and a more extensive field testing program with a wider range of variables is necessary.

A testing program designed to study how rock strength, discontinuity spacing, and discontinuity characteristics influence the rock mass performance during uplift failure would contribute significantly to our understanding of the problem. This program could be either a full-scale study or a controlled model study.

Appendix A

DETAILS OF FINITE ELEMENT STUDY

This appendix presents the details of the finite element study used to analyze the elastic stage of socket behavior. The results were presented in Figure 2-4. The study was a three-step process of generating the finite element mesh, applying the stresses and doing the analysis, and summarizing the results. The analyses were done using the general three-dimensional finite element code CIGAP, developed at Cornell University by Huang, Kulhawy, and Ingraffea (1).

The foundation was treated as an axisymmetric problem which allowed the three-dimensional problem to be analyzed from a two-dimensional mesh. The meshes for this problem were generated with the aid of a preprocessor and are presented in Figures A-1 and A-3. Figures A-2 and A-4 show the node numbers for the foundation elements and nearby elements in the rock mass.

Since the analysis was for uplift loading, there could be no stress transfer from tip resistance. To prevent the tip resistance, a soft zone one element thick was included beneath the foundation tip. This soft zone had a modulus of elasticity 1/20,000 the modulus of the foundation.

Changes in the stiffness ratio, $K_E = E_g/E_m$, were accommodated by changing the modulus of the rock mass from 2×10^9 through 2×10^{11} while the modulus of the foundation remained constant at 2×10^{10}. No units are associated with these numbers because only their relative magnitudes are important, provided that stresses are normalized in dimensionless form.

Load was applied to the foundation as a uniformly distributed surcharge acting upward across the foundation butt. Restraint against this load was provided by a combination of rollers along the bottom and two sides, and pins at the bottom and two outside corners as seen in Figures A-1 and A-3.

The axial stress distributions shown in Figure 2-4 were calculated from a weighted average of the vertical stress at the first six nodes starting at the centerline and working outward. The seventh node interfaces with the rock mass and was

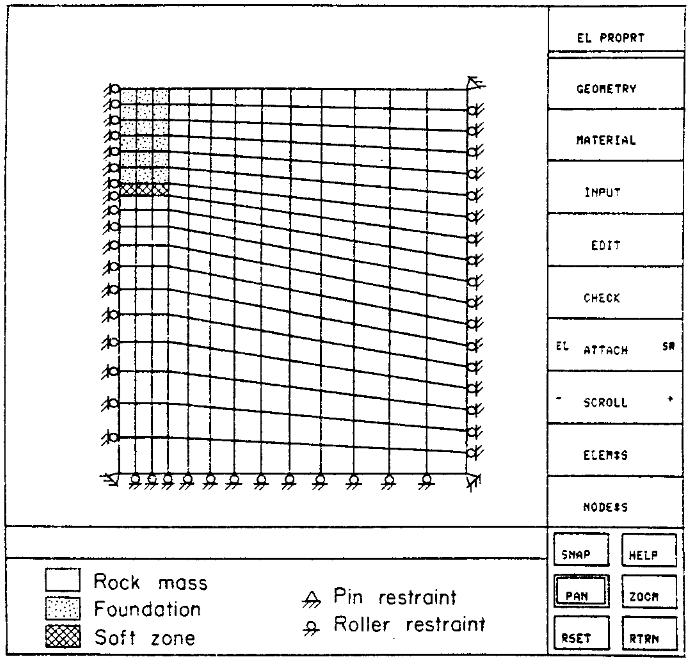

Figure A-1. Mesh for Socket with Length/Radius = 2.0

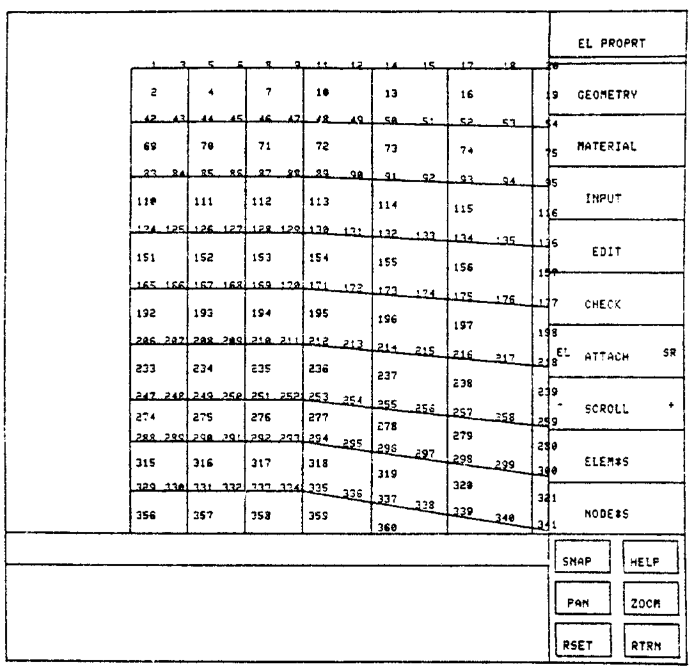

Figure A-2. Node Numbers for Socket with Length/Radius = 2.0

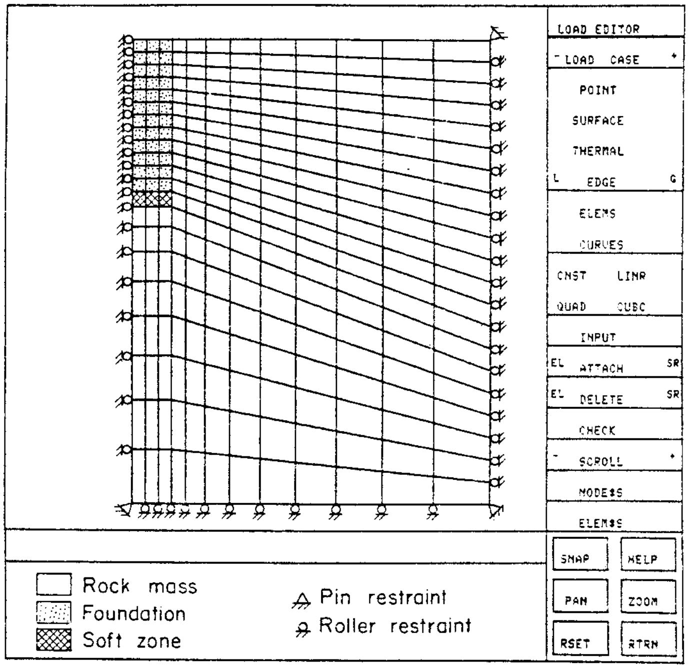

Figure A-3. Mesh for Socket with Length/Radius = 4.0

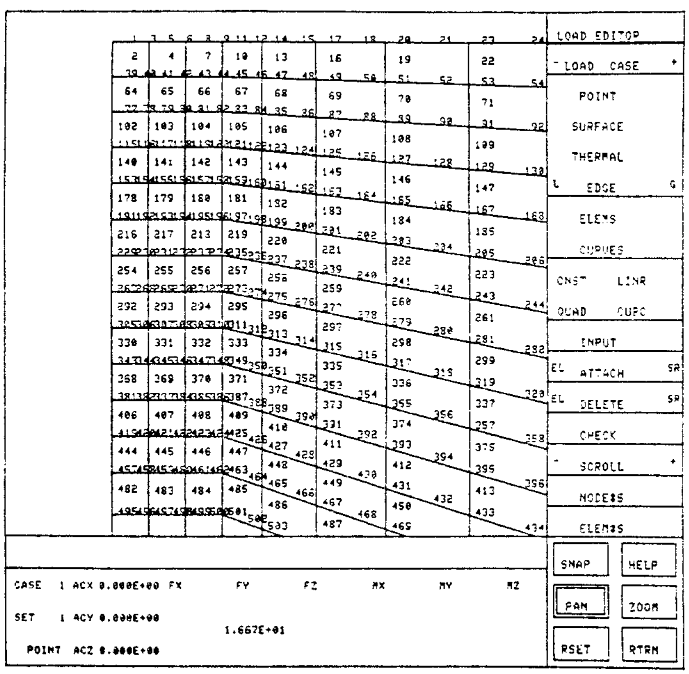

Figure A-4. Node Numbers for Socket with Length/Radius = 4.0

excluded from the calculations because it included vertical stress within the rock mass. The shear stress distributions were obtained from the nodes along the foundation-rock mass interface. The two nodes closest to the surface were not included because the shear stress increases then decreases rapidly in this region and the results are difficult to interpret. A finer mesh is necessary to study the near-surface stress distributions in more detail.

REFERENCE

1. Huang, Y.-P., Kulhawy, F. H., and Ingraffea, A. R., "Nonlinear, Incremental, 2-D and 3-D Finite Element Analysis of Geotechnical Structures Using Interactive Computer Graphics," Geotechnical Engineering Report 83-8, Cornell University, Ithaca, NY, Aug. 1983, 338 p.

Appendix B

PRESENTATION OF FIGURES SHOWING BEHAVIOR OF DIRECT SHEAR TESTS AND SOCKET LOAD TESTS

Appendix B presents the results of the analysis of constant normal stiffness (CNS) direct shear tests and socket load tests which were not included in Section 3. First are the figures for each of the CNS direct shear tests by Dight and Chiu (1). Two figures are presented for each test; the first shows the calculation of the empirical constant b, and the second compares the curve of best fit with the actual data. Following these are figures showing the dilations and shear stresses for the socket load tests by Williams (2). For each of these tests, two figures are presented. The first compares the modeled dilations with the back-calculated dilations, and the second shows the curve of best fit superimposed on the shear stress-displacement data.

REFERENCES

1. Dight, P. M. and Chiu, H. K., "Prediction of Shear Behavior of Joints Using Profiles," International Journal of Rock Mechanics and Mining Sciences, Vol. 18, No. 5, Oct. 1981, pp. 369-386.

2. Williams, A. F., "Principles of Side Resistance Development in Rock Socketed Piles," Proceedings, 3rd Australia-New Zealand Conference on Geomechanics, Vol. 1, Wellington, 1980, pp. 87-94.

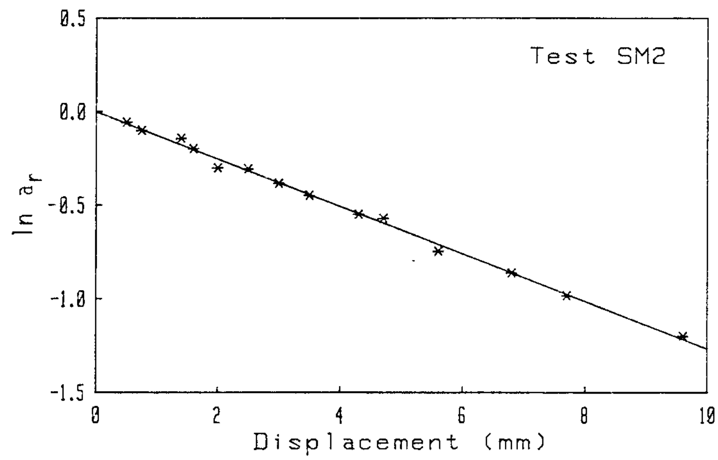

Figure B-1. Determination of k_1 for Test SM2

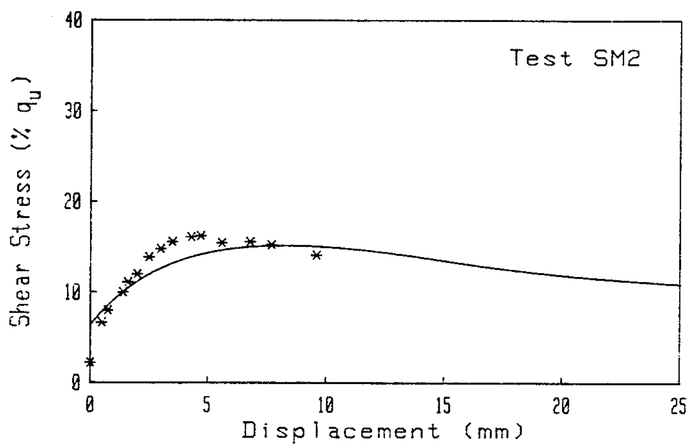

Figure B-2. Shear Stress-Displacement Curve of Best Fit for Test SM2

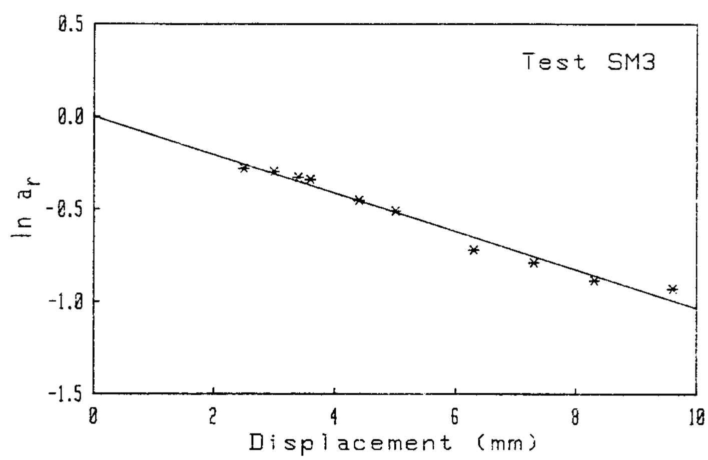

Figure B-3. Determination of k_1 for Test SM3

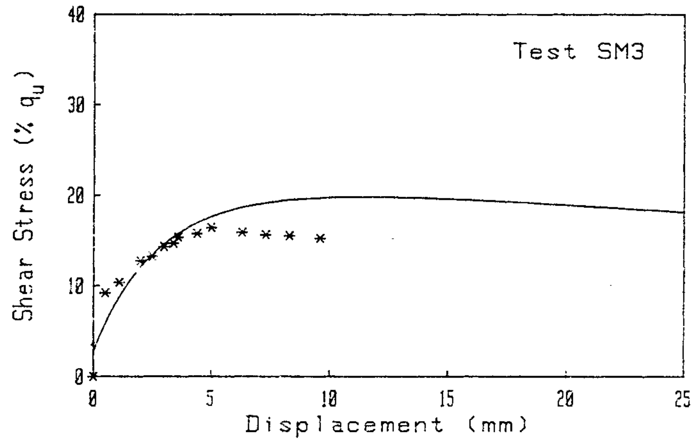

Figure B-4. Shear Stress-Displacement Curve of Best Fit for Test SM3

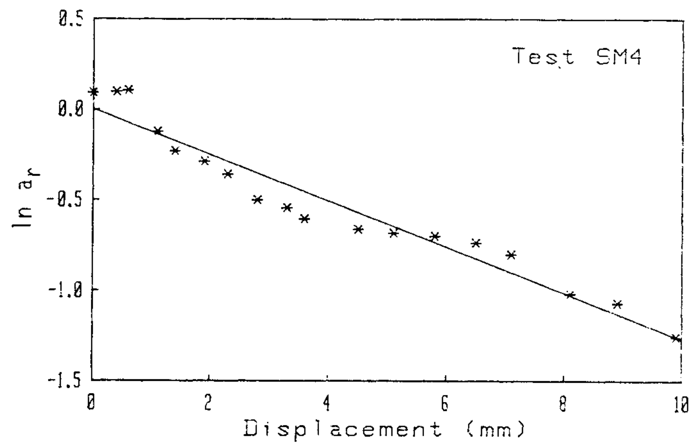

Figure B-5. Determination of k_1 for Test SM4

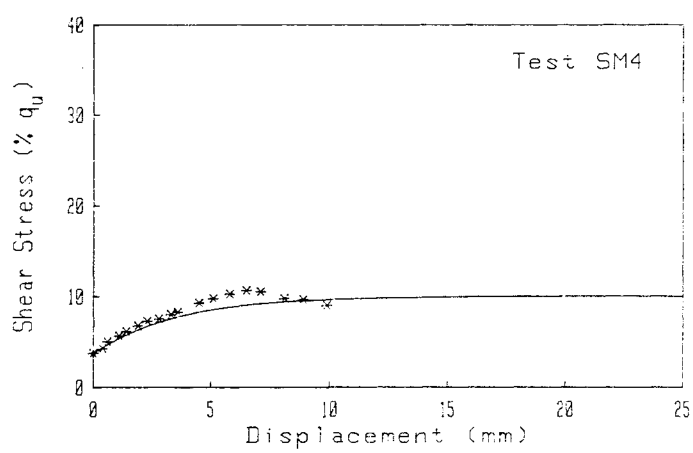

Figure B-6. Shear Stress-Displacement Curve of Best Fit for Test SM4

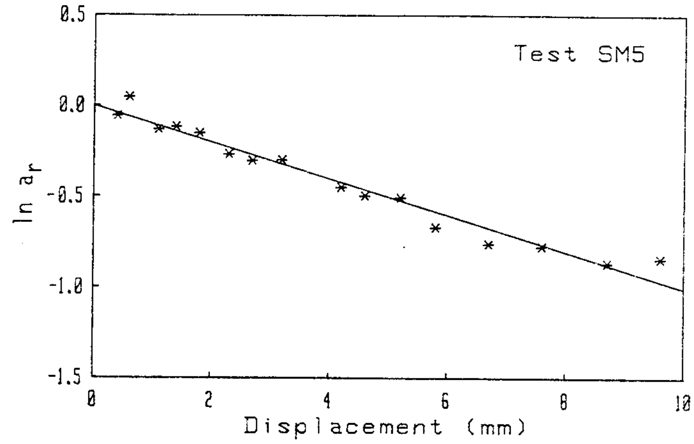

Figure B-7. Determination of k_1 for Test SM5

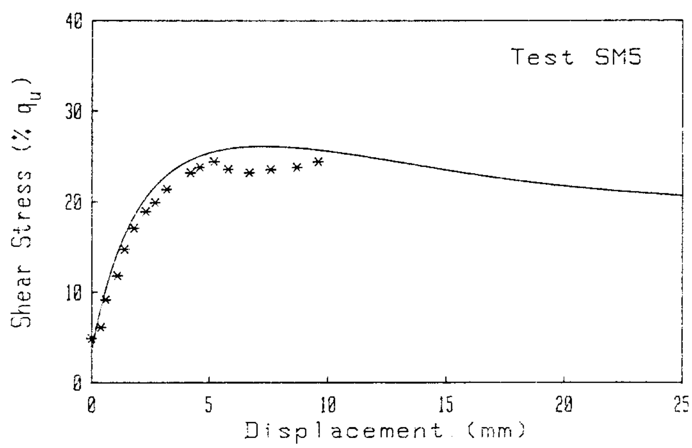

Figure B-8. Shear Stress-Displacement Curve of Best Fit for Test SM5

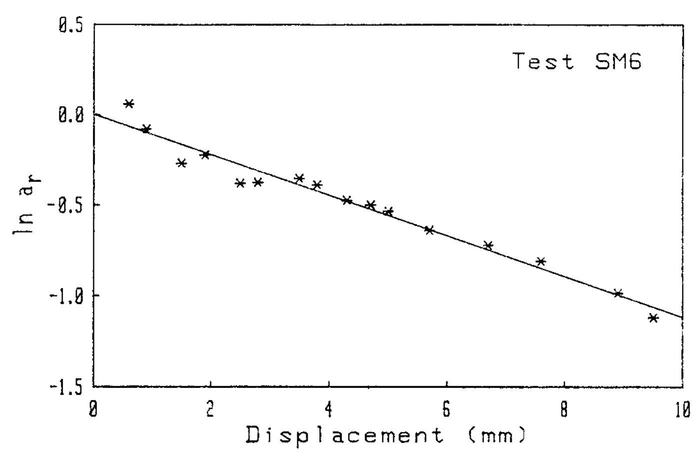

Figure B-9. Determination of k_1 for Test SM6

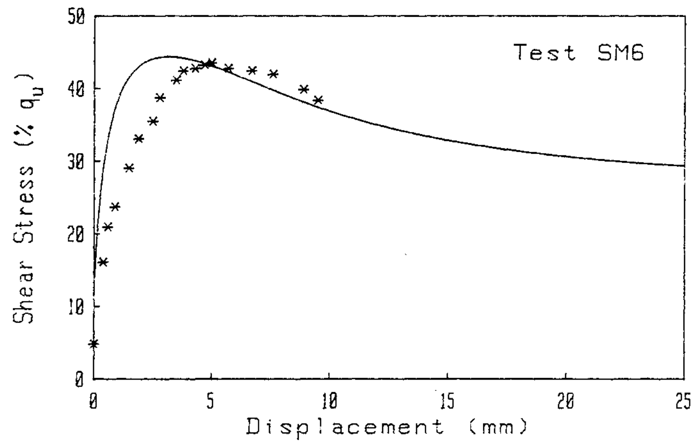

Figure B-10. Shear Stress-Displacement Curve of Best Fit for Test SM6

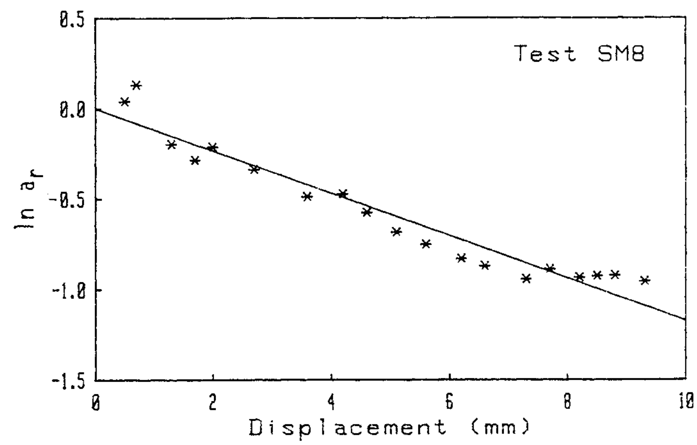

Figure B-11. Determination of k_1 for Test SM8

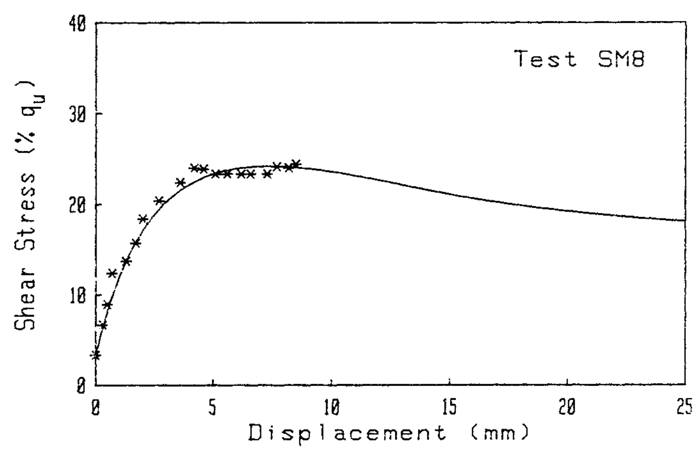

Figure B-12. Shear Stress-Displacement Curve of Best Fit for Test SM8

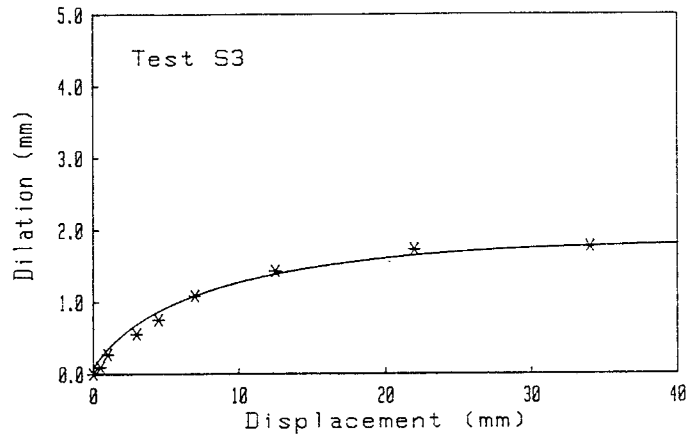

Figure B-13. Modeling Dilations for Shear Socket S3 Using Equation 3-1

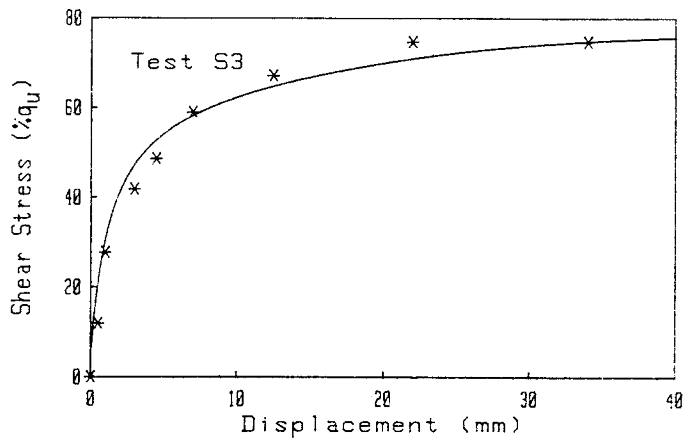

Figure B-14. Shear Stress-Displacement Curve of Best Fit for Shear Socket S3

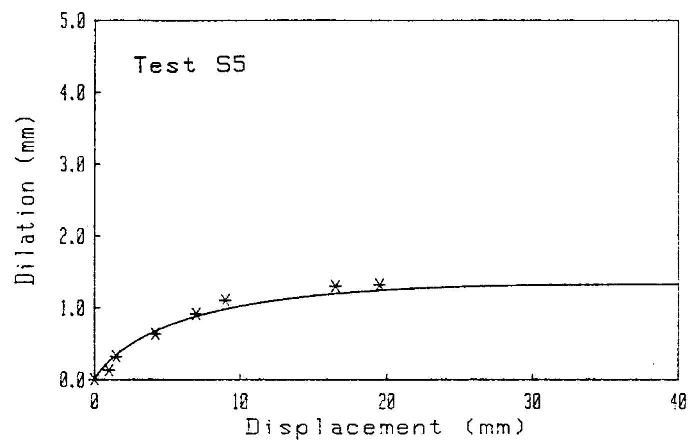

Figure B-15. Modeling Dilations for Shear Socket S5 Using Equation 3-1

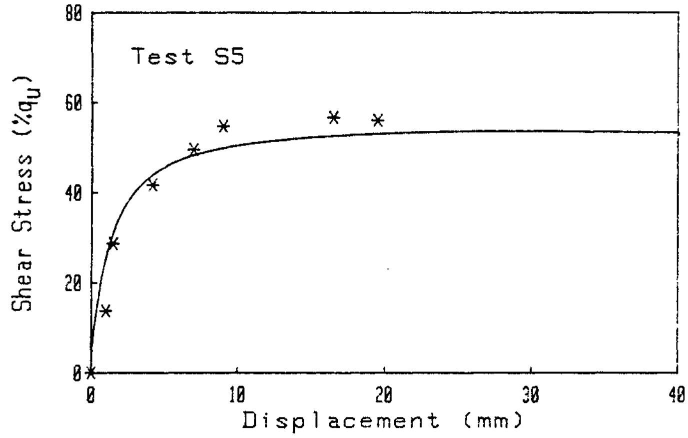

Figure B-16. Shear Stress-Displacement Curve of Best Fit for Shear Socket S5

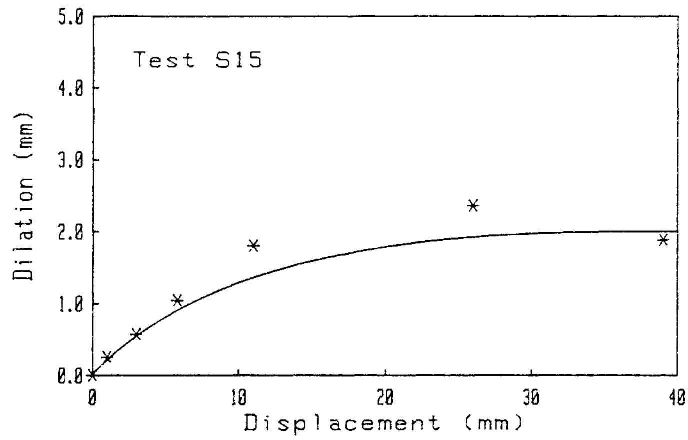

Figure B-17. Modeling Dilations for Shear Socket S15 Using Equation 3-1

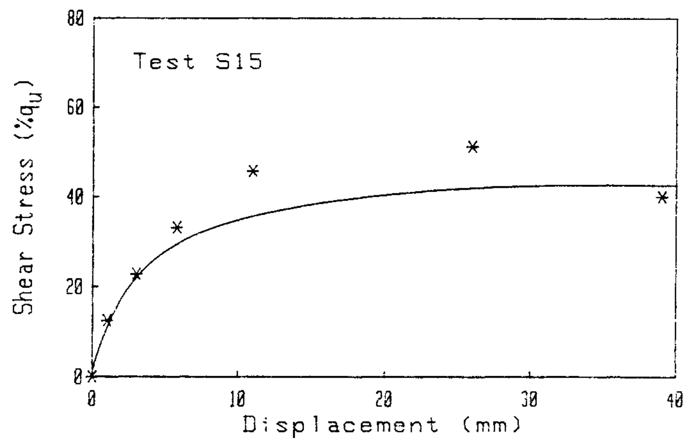

Figure B-18. Shear Stress-Displacement Curve of Best Fit for Shear Socket S15

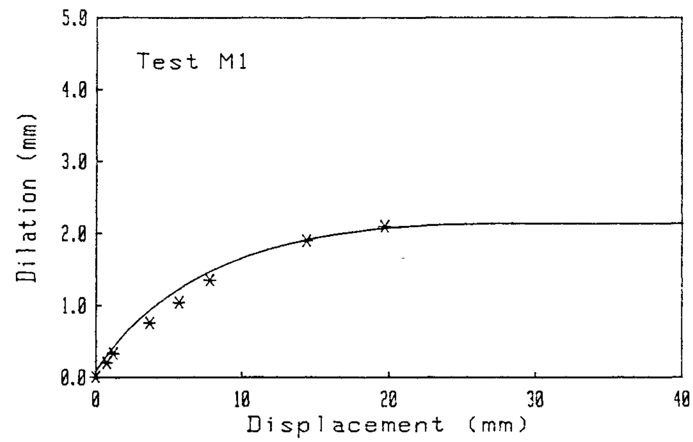

Figure B-19. Modeling Dilations for Shear Socket M1 Using Equation 3-1

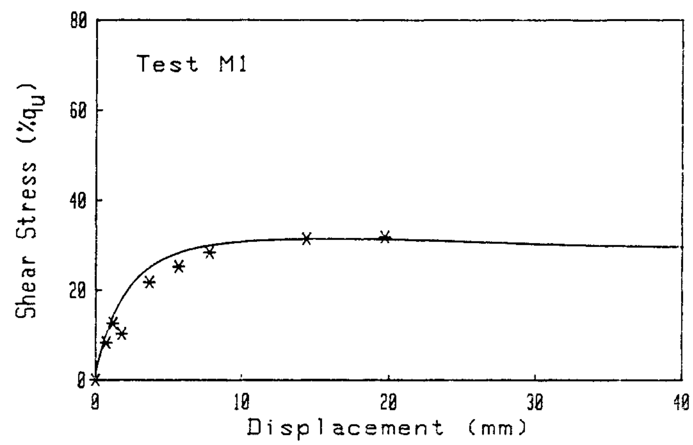

Figure B-20. Shear Stress-Displacement Curve of Best Fit for Shear Socket M1

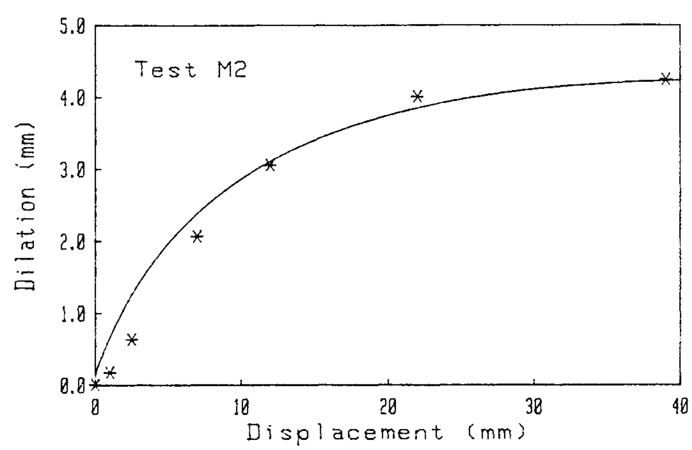

Figure B-21. Modeling Dilations for Shear Socket M2 Using Equation 3-1

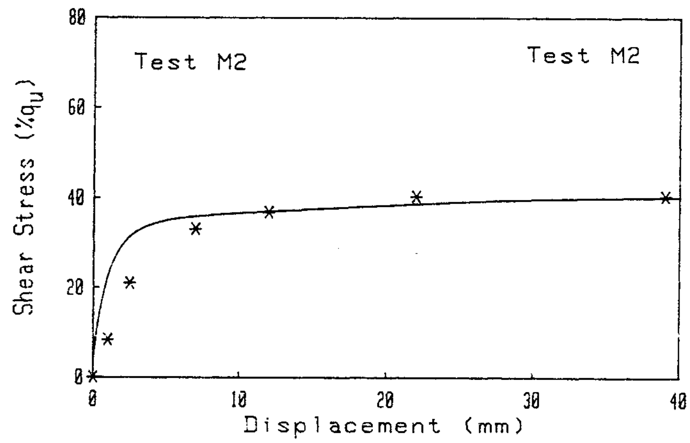

Figure B-22. Shear Stress-Displacement Curve of Best Fit for Shear Socket M2

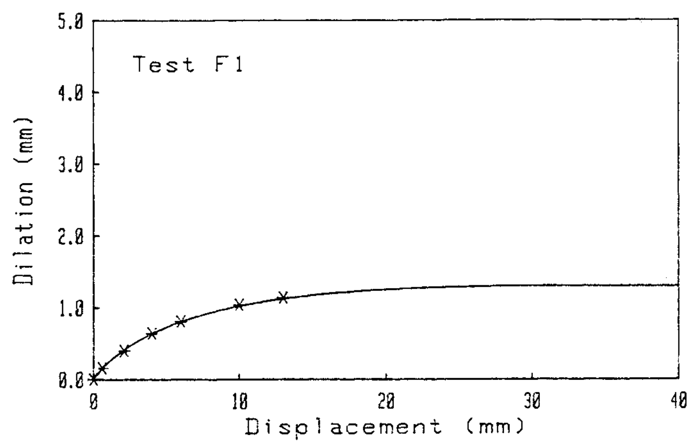

Figure B-23. Modeling Dilations for Shear Socket F1 Using Equation 3-1

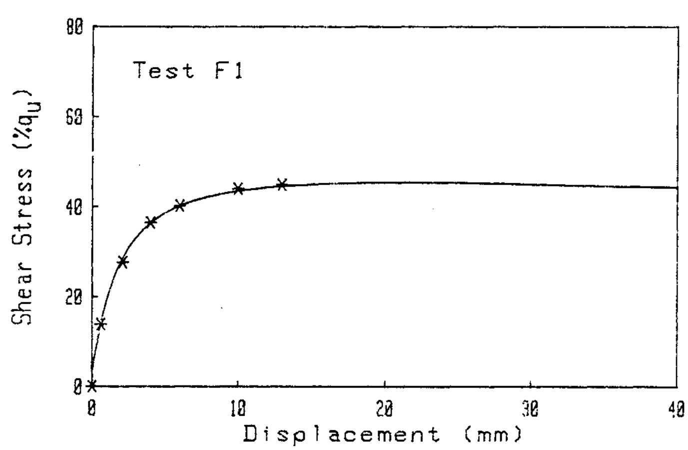

Figure B-24. Shear Stress-Displacement Curve of Best Fit for Shear Socket F1

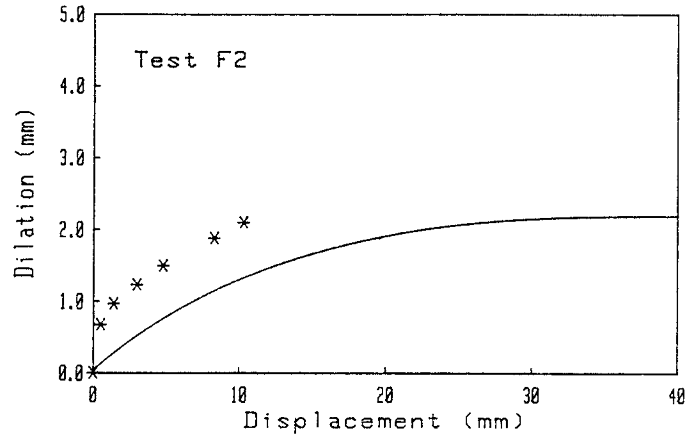

Figure B-25. Modeling Dilations for Shear Socket F2 Using Equation 3-1

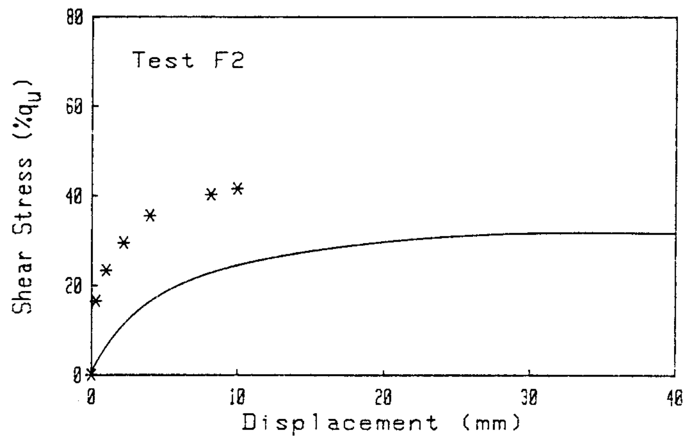

Figure B-26. Shear Stress-Displacement Curve of Best Fit for Shear Socket F2

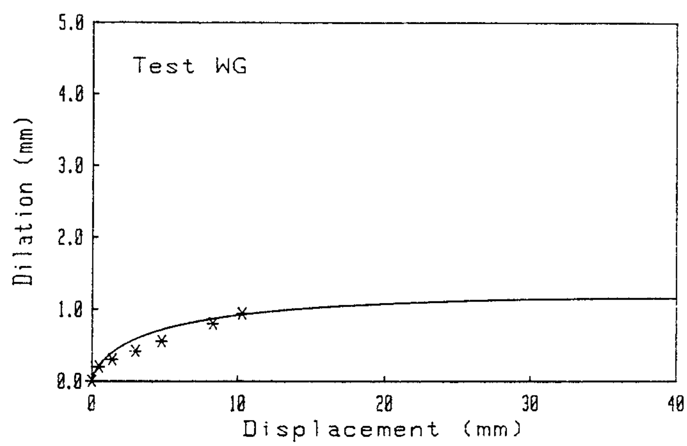

Figure B-27. Modeling Dilations for Shear Socket WG Using Equation 3-1

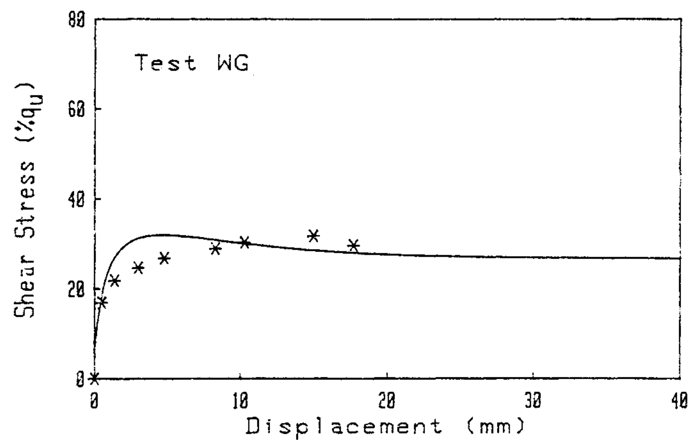

Figure B-28. Shear Stress-Displacement Curve of Best Fit for Shear Socket WG

About EPRI

EPRI creates science and technology solutions for the global energy and energy services industry. U.S. electric utilities established the Electric Power Research Institute in 1973 as a nonprofit research consortium for the benefit of utility members, their customers, and society. Now known simply as EPRI, the company provides a wide range of innovative products and services to more than 1000 energy-related organizations in 40 countries. EPRI's multidisciplinary team of scientists and engineers draws on a worldwide network of technical and business expertise to help solve today's toughest energy and environmental problems.

EPRI. Electrify the World

Printed on recycled paper in the United States of America

EPRI • 3412 Hillview Avenue, Palo Alto, California 94304 • PO Box 10412, Palo Alto, California 94303 • USA
800.313.3774 • 650.855.2121 • askepri@epri.com • www.epri.com